Simulation of a Solid Rocket Exhaust System

Nuno Miguel Pereira da Cruz Rosário

Dissertação para obtenção do Grau de Mestre em

Engenharia Aeroespacial

Júri

Presidente:	Prof. Doutor Fernando José Parracho Lau (IST–DEM)
Orientador:	Prof. Doutor José Carlos Fernandes Pereira (IST-DEM)
Orientador Externo:	Doutor Neil Paul Murray (ESA-ESTEC)
Vogal:	Prof. Doutor João Manuel Melo de Sousa (IST-DEM)

Novembro 2012

RESUMO

A mistura utilizada em motores de foguete de combustível sólido incorpora na maioria dos casos, pequenas partículas metálicas com o objetivo de aumentar a temperatura da combustão e a sua estabilidade. Estas partículas têm no entanto alguns efeitos adversos na pluma de gases de escape que sai para a atmosfera. Neste trabalho foram estudados esses efeitos através da simulação numérica e os cálculos foram efetuados através do código comercial FLUENT®. Verifica-se de um modo geral a existência de um grande aumento da temperatura global da pluma bem como uma diminuição da sua velocidade. Esta análise foi uma análise qualitativa que permitiu comparar vários tamanhos de partículas e dois tipos de distribuição das mesmas. Estas variações nas características das partículas produziram resultados diferentes entre elas. Foram também observadas diferenças significativas a nível físico e numérico fazendo variar a pressão atmosférica e a temperatura ambiente (altitude). Os cálculos produziram alguns erros numéricos que foram analisados ao longo do trabalho e foram apresentados futuros desenvolvimentos com soluções para os problemas encontrados.

Palavras-chave: Motores de foguete; Interação de partículas; Escoamento multifásico; Plumas de foguetes.

ABSTRACT

The propellant mix used in solid rocket motors often includes small metallic particles in order to increase the combustion temperature and stability. However, these particles tend to have adverse effects on the gaseous exhaust plume that leaves the rocket into the atmosphere. In this work, those effects have been studied numerically by the commercial code FLUENT®, and an increase in the plume temperature was found, together with a hard deceleration of the exhaust flow allowing characterizing several particle sizes as well as two different types of distribution. These changes in the particles' properties were found to provide significantly different results. There were also observed several important physical and numerical changes by varying the ambient pressure and temperature (altitude). Several numerical errors were also found due to the presence of a rarefied flow area and possible solutions for the problems found are presented.

Keywords: Solid rocket motor; Particle interaction; Multiphase flow; Rocket plume.

ACKNOWLEDGMENTS

First of all I'd like to thank the ESTEC TEC-MPA section head Dr. José Longo, for the opportunity he gave me to work on his section, without which this work would never have been possible. I would also like to thank my ESTEC supervisor Dr. Neil Murray for all his orientation, help and availability throughout the whole work, and the whole TEC-MP division for the good times spent during those 6 months. I'd like to mention Dr. Henry Wong from ESA/AOES and Dr. Richard Schwane from ESTEC, who firstly proposed me this work and provided the initial insight to the problem in study.

I'd also like to thank my IST supervisor for accepting to help me with the thesis, Prof. José Carlos Pereira, and the whole IST staff that lectured me and helped me finish the course.

On a more personal way, I need to thank my whole family for supporting me through the entire course and for the sacrifices they made to allow me to go to the Netherlands. Hope this work makes them proud.

Finally, I'd like to thank all my close friends who supported me during my highs and lows as I made this thesis, without whom I'd never be able to find the right way to proceed.

Thank you all.

NOMENCLATURE

Compressible Flows

m	Mass
ρ	Density
M	Mach number
γ	Specific heat ratio
R	Gas constant
T	Temperature
$\mathbf{F}$	Net force
$\mathbf{f}$	Body force per unit mass
$\mathbf{V}$	Velocity vector $\mathbf{V} = (u, v, w)$
p	Pressure
σ_{ij}	Stress tensor
τ_{ij}	Shear stress tensor
μ	Kinematic viscosity
h	Enthalpy
k	Thermal conductivity
S	Heat source term

Nozzle Theory

c_v	Specific heat for constant volume
c_p	Specific heat for constant pressure
T	Temperature
R	Gas constant
$\mathcal{R}$	Universal gas constant
T	Temperature
n	Number of moles
ρ	Density
h	Enthalpy
e	Energy per unit mass
u	Fluid axial velocity

h_0 Total/stagnation enthalpy

T_0 Total/stagnation temperature

p_0 Total/stagnation pressure

ρ_0 Total/stagnation density

A Area

M Mach number

A_e Nozzle exit area

M_e Nozzle exit Mach number

A_t Throat area

p_i Nozzle inlet pressure

p_e Nozzle exit pressure

h_i Nozzle inlet enthalpy

h_e Nozzle exit enthalpy

$\dot{m}$ Mass flow rate

p_a Ambient pressure

v_e Exhaust velocity

V_{eff} Effective exhaust velocity

I_{sp} Specific impulse

C_F Thrust coefficient

g Gravitational acceleration $g = 9.81\ m/s^2$

Particle Force Calculation

$\mathbf{F}_D$ Drag force exerted on the particle

$\mathbf{F}_P$ Pressure force exerted on the particle

$\mathbf{F}_G$ Gravitational force exerted on the particle

$\mathbf{F}_X$ Other forces exerted on the particle

$\mathbf{V}_p$ Particle velocity

$\mathbf{V}_f$ Fluid velocity

$\mathbf{V}_{f0}$ Initial fluid velocity

ρ_p Particle density

ρ_f Fluid density

m_p Mass of the particle

$\mathcal{V}_p$	Particle volume
S	Particle surface area $S = \pi d_p^2$
d_p	Particle diameter
C_D	Drag coefficient
Re	Reynolds number
μ_f	Fluid dynamic viscosity

Rarefied Flows

Kn	Knudsen number
λ	Mean free path
L	Characteristic length
Re	Reynolds number
M	Mach number

Thrust Estimation

F_{throat}	Force in the thrust plane
F_{exit}	Force in the exit plane
F_{net}	Net thrust

LIST OF FIGURES

LIST OF TABLES

LIST OF CHARTS

TABLE OF CONTENTS

1. INTRODUCTION AND BACKGROUND

1.1. Motivation

The propellant mix used on solid rocket motors to produce thrust is generally composed by a large percentage of a crystalline oxidizer (usually some form of ammonium perchlorate), a metallic powder (aluminium) and a polymeric binder. The addition of the metallic particles increases combustion stability and temperature, but it comes with some disadvantages for the gaseous plume that leaves the rocket. The main worry is that this increase in combustion temperature will lead to an overall raise in the plume temperature which, together with the solid particles, can provoke larger emission of radiation in high-altitude and wide opened plumes, possibly affecting the cargo payload and therefore damaging it. For this reason, this study should provide a general idea of what temperatures to expect in the plume and what is the effect of having solid metallic particles in the plume, allowing for a future estimation of the amount of radiation received by the payload and for a better prediction of this damage.

On the other hand, the aluminium particles also decelerate the flow, as it will be shown throughout this work, leading to a decrease on the rocket performance. This work will analyse the variations on the thrust that comes with the addition of solid particles on a gaseous flow under a number of ideal conditions that can afterwards be extrapolated to more realistic scenarios.

The amount of aluminium added to the fuel is therefore function of all these effects and there is an optimum value that maximizes performance.

It is important to refer that this study is a qualitative analysis which allows an understanding of the processes that are impacted by the particles, not providing an accurate quantification of the actual impact due to uncertainties on the particle size and distribution and due to the inaccuracy of some of the numerical solvers used for this kind of flow.

1.2. Solid Rocket Motors

1.2.1. Solid Rocket Motors Fundamentals

Rocket propulsion systems can be classified according to the type of energy source they use: chemical, nuclear, electric or solar. In the chemically based propulsion systems, energy comes from a high-pressure combustion process, where the reacting fuel and oxidizer produce very high temperature gases (2700 to 4300 K) [1]. These gases are then expanded through a nozzle, where they are accelerated to very high velocities before leaving the system. In this category we may distinguish three main types of engines: solid propellant motors, liquid propellant engines or hybrid (liquid and solid) propellant systems. Gaseous propellant engines are also available, however they don't have as much use as the ones presented before.

In the past decades, liquid rocket engines have been used for the most common applications in space propulsion, in particular, in space launchers or boosters. These systems provide a high specific impulse and a good throttling capability and that made them a regular choice for rocket designers. However, as everything on this field, this comes with a high production cost and with a more challenging design and test process.

Liquid propellants need additional storage tanks and a feeding mechanism which greatly increase their complexity. The storage of liquid propellants can't be done for a long period of time, and should be done very carefully to avoid leaks, as these propellants can be hazardous, toxic and/or corrosive.

Solid rocket motors (SRM) have been used since before the 20th century. The research on the liquid engines reduced their applications, but nowadays these systems are still used in a variety of projects. The SRM are usually simpler and easier to operate than the liquid propellant engines and that makes them top choice for a wide range of applications, including satellite positioning boosters and launchers. Their storage is usually safer and they last longer than liquid propellants.

A SRM system is usually composed only by a combustion chamber, where the solid fuel is stored and combusted, and a convergent-divergent nozzle, responsible for the acceleration of the gaseous combustion products, as shown in Figure 1. We should note that, unlike the liquid-based engines, most SRM don't have moveable parts and require fewer sub-systems included (liquid ones for example, need temperature control systems and fuel pumps).

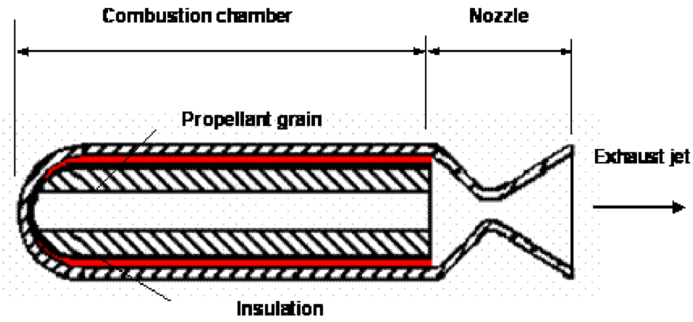

Figure 1 – Solid rocket motor scheme (image from http://www.lr.tudelft.nl)

1.2.2. Solid Propellants

The propellants used on high-altitude rocket motors, especially for large boosters and second stage motors need to satisfy a list of desirable characteristics in order to obtain their maximum performance. The main properties are listed below [1]:

- High performance or high specific impulse – high temperature and/or low gas molecular mass.
- Predictable and initially adjustable burning rate.
- Low burning rate and temperature coefficients.
- Adequate physical properties for the desired temperature range.
- High density (to reduce the motor volume).
- Desirable aging characteristics.
- Simple, low-cost and safe manufacturing.
- Low technical risk.
- Nontoxic exhausts.
- Not prone to combustion instability.

The propellants can be classified according to several parameters like their composition, application, density of the resulting smoke and toxicity. They can be divided in two main classes: double-based (DB) and composite.

Double-based propellants are made of a homogeneous mixture of a propellant grain and a solid fuel which absorbs liquid nitro-glycerine. These types of propellants have nearly smokeless and nontoxic exhausts and are used on small tactical missiles and other designs. They are mostly cheaper but have lower performance and density, which makes them worse for high-altitude rocket applications.

Composite propellants are composed by a heterogeneous mixture of oxidizer crystals (like ammonium perchlorate – AP) and a powdered metallic fuel (usually aluminium) held together by a liquid polymeric or plastic binder that acts like a structural glue.

Composite propellants can be divided into conventional, modified, high-energy and lower-energy propellants. Conventional propellants are composed by 60-72% AP, 22% aluminium (Al) and 8-16% of a binder (usually HTPB – hydroxyl-terminated polybutadiene). In order to increase the performance and the density of the propellant, sometimes energetic nitramines or plasticizers are added, leading to the modified composite propellants. Some other options can be taken by replacing the oxidizer by a nitrate or the binder by energetic materials, thus increasing or decreasing the energy released by the propellant.

The composite propellants are shown to have several advantages for high-altitude rocket applications. They provide a higher specific impulse, consequence of their higher density, and wider burning rates. Figure 2 (taken from [1] and adapted from [2]) shows a comparison between the burning rate interval and specific impulse for several types of solid propellants.

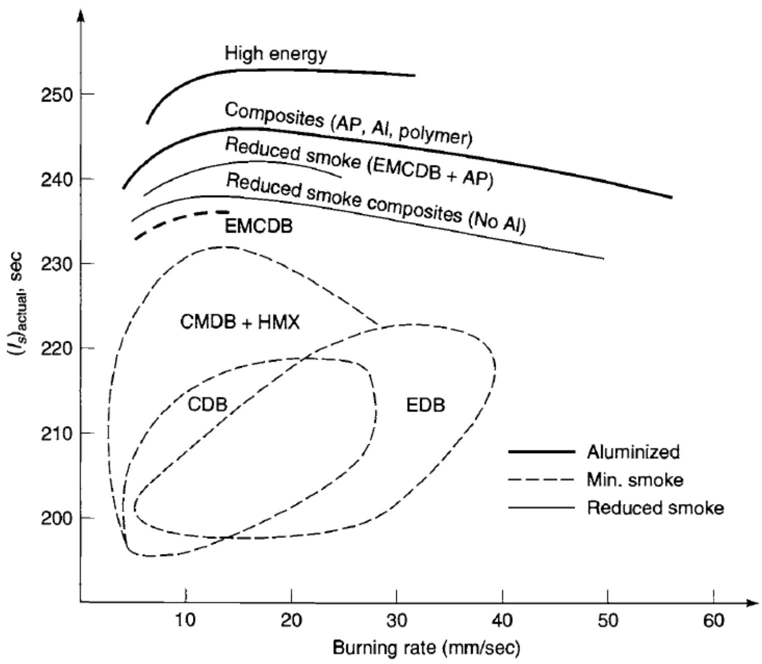

Figure 2 – Typical delivered specific impulse and burning rate for several solid propellant categories. (Image credit to [1] [2])

Comparing the several types of propellant for the same burning rate we find that the absence of aluminium reduces the specific impulse, while the high-energy composite materials have it at higher values. To quantify these variations, the figure shows that the estimated specific impulse at standard conditions for a burning rate of 30 mm/sec is 245 sec for conventional composites, reaching 235 sec (4% lower) without aluminium (reduced smoke) and more than 250 (2-3% higher) for the high-energy propellants. It can be seen that the composite propellants have almost the same performance and density. As a remark, the figure also shows that the double base propellants have significantly lower values for the specific impulse and a more narrow range of burning rates.

The aluminium introduced in the fuel can be quite hazardous despite the combustion performance increase it provides. During the combustion, the aluminium powder is oxidised to aluminium oxide, which forms visible and toxic smoke particles in the exhaust plume. For this reason, most composite propellants are smoky, unlike the double-based propellants.

Data from reference [1] shows that an increase in the metallic content of the fuel leads to an increase of the flame temperature. It is also shown that propellants with AP and Al provider higher specific impulses than other oxidizers and fuels.

The most common conventional composite propellants use CTPB (carboxyl-terminated polybutadiene) or HTPB (hydroxyl-terminated polybutadiene) as the binder for the solid ingredients. Between these two, HTPB provides a better solid loading percentage, and therefore, performance as well as a wider ambient temperature range and burning rate range. It is important to notice that the highest performance is achievable by replacing the HTPB for an energetic binder like HMX (cyclotetramethylenetetranitramine). This alternative is far more expensive that the conventional one and therefore it is seldom used.

Let’s now consider a composite propellant with HTPB as a binder and check the effect of the other two main components in the overall performance of the propellant. Data from [1] and [3] show that both the specific impulse and the flame temperature reach a maximum for 93% AP (ammonium perchlorate) oxidizer concentration. AP is shown to have the highest specific impulse of all the common oxidizers for the same concentration and is therefore the most common one. Due to the presence of other solids like aluminium, it is impossible to reach the optimum concentration in a propellant mix.

From the several oxidizers already tested in solid rocket propulsion, ammonium perchlorate is the most used by far. It has the highest specific impulse and it is easy to handle. For these reasons, AP tends to increase its use even more in the future. Other oxidizers include potassium perchlorate (KP) and nitrates. Nitrates can be used despite their lower performance since they are cheaper and smokeless.

The solid metallic fuels (with aluminium being the most common) usually consist of small spherical particles (5 to 60 μm diameter), and they constitute from 14 to 20% of the propellant. The metallic particles increase the combustion temperature as well as the specific impulse and the amount of heat generated. However, the aluminium fuel has several disadvantages for the combustion process as it changes phase and oxidizes during the combustion, leaving a toxic exhaust in the plume. Boron and beryllium are other options to use as a fuel, each one with their own pros and cons. Boron has a higher melting point but it difficult to burn efficiently, while beryllium improves the specific impulse but its oxide is far more toxic than aluminium's.

Knowing the conventional composition of a solid propellant, reference [4] provides a study of several propellants to show the optimum composition of the mixture which gives the maximum specific impulse. Considering a propellant with AP and Al, the optimum percentages of each one are usually around 72% and 16% respectively [4].

1.3. VEGA Launcher

VEGA (*Vettore Europeo di Generazione Avanzata* – European Advanced Generator Carrier Rocket) is an expendable launch vehicle developed by the European Space Agency and the Italian Space Agency.

Earth observation missions take place in polar or low earth orbits, and for that there is a need for an economic way to put the respective satellites in orbit. VEGA was developed with the aim of satisfying those needs, covering a wide range of missions and payload configurations. It is capable of putting multiple payloads in orbit at the same time and covers a wide range of payload mass.

Height	30 m
Diameter	3 m
Lift-off mass	137 tons

Table 1 – VEGA launcher main characteristics (from http://www.esa.int)

VEGA propulsion system is constituted by a total of four stages: three solid-propellant stages and a liquid-propellant upper module for attitude control and satellite release. The solid motor stages can be split as:

- **First stage:** The booster stage is constituted by a P80 solid-propellant motor developed by Avio containing about 88 tons of propellant and achieving a net thrust of 3 040 kN. It operates at a chamber pressure of 95 bar and has an expansion ratio of 16.
- **Second stage:** The second stage of the VEGA launcher is a Zefiro 23 solid-propellant motor. This motor fires after the first one and operates under a chamber pressure of 106 bar, allowing it to reach a thrust of 1 200 kN. Its area ratio is 25.
- **Third stage:** The third solid motor in VEGA is the Zefiro 9. It has a chamber pressure of 74 bar and an expansion ratio of 56, being the largest of all three stages. It achieves a thrust of 313 kN.

1.4. Background Developments

Over the last decades the number of studies of solid rocket exhaust plumes has been increasing, due to a need of a constant search for improved models, solutions and strategies. We can divide these studies in three categories: those that analyse the behaviour of the two-phase flow through the nozzle and the interaction between the two phases, those that estimate the particle size distribution on the nozzle, and those that focus on the plume development and its behaviour.

1.4.1. Two-phase Flows in Nozzles

Retrieving the correct flow behaviour from the combustion chamber and through the nozzle plays a fundamental role in the overall plume analysis, as the nozzle exit conditions act as an input condition for the plume. Therefore, without an accurate modelling of the flow in the nozzle, it is impossible to obtain correct results for the plume properties. Getting the flow properties inside the motor requires a good understanding and a good modelling of the interaction between the flow and the particles.

Computational and analytical treatments of two phase nozzle flows were reviewed by Burt [5] and can be divided in several categories.

Quasi-one-dimensional approaches have been used for some time [6] and although they don’t provide boundary layer information, they are often inexpensive, provide an easy access to two-way coupling and allow the introduction of other physics models. One of the simplifying assumptions of this theory is that the flow is isentropic and chemically frozen. In one of the earlier studies, Bailey *et al*. (1961) [7] used this approach to calculate the gas flow and then used a post-processing approach to model the trajectories and temperatures of the particles through the nozzle. Matsuzaki (1988) [8] applied the quasi one dimensional model to calculate a flow on a nozzle considering chemical and thermal non-equilibrium, providing a simplifying method to study these particular kind of complex aerodynamic flows.

The method of characteristics [9] is a more accurate numerical technique but also has some limitations. It is based on the mathematical characteristics of the governing equations. Since it only works for hyperbolic equations, it needs to be used in the supersonic divergent part of the nozzle or for the unsteady form of the Euler equations that are hyperbolic for low and high speed flows. This method doesn't take into account viscosity effects (i.e., the flow is assumed to be inviscid), hindering the accuracy of the calculation.

To overcome these limitations, more recently new models were developed. Eulerian schemes were used by Chang [10] to compute both the gas and particle phases, allowing a better coupling between them and therefore a more accurate solution. This approach requires a low amount of computational memory which makes it a good way to save computation time. Although chemical reactions are still not taken into account, particle heat loss and velocity change are incorporated in the Eulerian model. Various particle sizes and geometries were analysed over several complex geometries, including the chamber and the nozzle of the IUS Small SRM – Figure 3.

Figure 3 – IUS small motor

The standard disperse (gas-solid) two-phase flow modelling approaches – Eulerian-Eulerian or Eulerian-Lagrangian simulations – can be used for the solid rocket exhaust plumes. Hwang and Chang [11] presented a study based on a Lagrangian tracking scheme to get the particle influence of the flow. This allowed them to evaluate the particle source terms and apply them to the one-phase gas flow solution previously computed through an Eulerian approach.

1.4.2. Particle Size

In order to obtain the influence of the solid particles on the nozzle gaseous flow, it is fundamental to know the particle size and their distribution. The particle distribution in the chamber is one of the most difficult parameters to model since there is poor knowledge and limited experimental data. Despite this, several trials were made to develop theoretical models that show the size distribution of the particles. One approach that is made is to determine a correlation that relates the particle size to the nozzle and propellant variables, with the advantage of being directly documented by experiments. This can be seen in reference [12], where there were made comparisons between the predicted sizes and the measured ones for several motors. In that particular example, smaller particle sizes tend to be more accurately predicted. The maximum error found was 17%. Another approach is based on the critical Weber number[1] as studied by Morrell [13].

Hermsen [14] reviewed in his paper both of these approaches and several models developed in order to study the particle growth in the chamber and the nozzle. It was shown that the throat diameter was the most important variable influencing the particle size (Figure 4), although smaller effects of chamber pressure and aluminium concentration were also found.

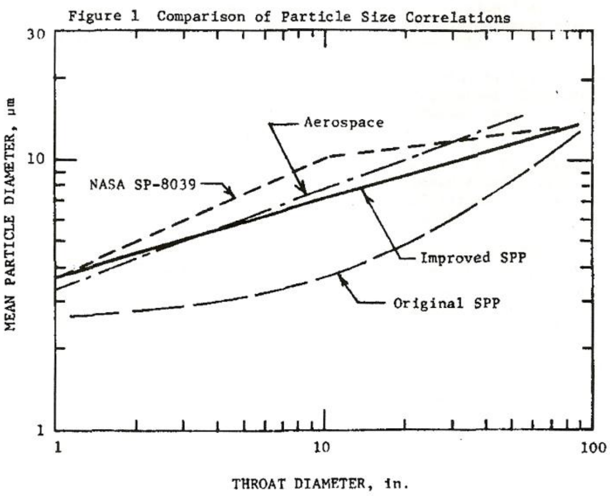

Figure 4 – Comparison of Particle Size Correlations from reference [14].

[1] The Weber number can be seen as a measure of the relative importance of the fluid's inertia compared to its surface tension. It is an important parameter on multiphase flows and droplet formation.

According to Hermsen [14], Fein's theoretical model [15] is found to be accurate to predict the size of the particles on the chamber, but it needs the mean particle size as an input, making it unsatisfactory on its own. Using the average size of the experiments, this correlation successfully estimated the size distribution up to five orders of magnitude in the particle volume. Jenkins and Hoglund [16] model also obtains good agreement between experimental and theoretical data utilizing a generalised form of the kinetic-coagulation equation and checking the dependence of the collisions and the condensation. This model predicts an exponential distribution along the rocket motor, showing dependence on the particle diameter and concentration. It is also shown that condensation is the main factor on the chamber, while collisions are the main growth criteria on the nozzle itself. In this region, acoustic effects and condensation only vary 8-16% of the diameter. As for the growth in the nozzle there were also studies from Marble [17] and Nack [18] that assumed a constant fluid-particle velocity lag, leading to the conclusion that the throat diameter doesn't influence the particle growth in the nozzle. However, Crowe and Willoughby [19] later showed that for a non-constant velocity lag, the throat diameter had some influence on that same particle growth.

1.4.3. Continuum Model for High-altitude Plume Simulations

The simulation of high-altitude plumes is more complicated and challenging due to the rarefied properties of the flow. The continuum model based on the Navier-Stokes equations is not valid for high Knudsen numbers and therefore different techniques like the DSMC (Direct Simulation Monte Carlo Method) [5] are used. The continuum method assumes thermal equilibrium at one temperature while the DSMC method is able to capture the thermal non-equilibrium of rarefied and high-gradient flows, which are caused mainly by the low pressure and the high velocities. The continuum model also assumes a Maxwellian distribution for the molecule velocity which is not true for rarefied flows. These faults were investigated by other studies [20] [21] which provided a comparison between the continuum-based method and the DSMC method. Boyd et al. [21] showed that although the continuum model can be used for industrial applications, the DSMC method is more accurate at reproducing the results obtained by experimental analyses. The same conclusions were reached by Selezneva et al. [20] who found that the continuum model produced satisfactory resemblance to the experimental fluid temperature and velocity. However it is also added that the CFD results can be doubtful and require validation from experimental data. The DSMC method was found to be ineffective for the nozzle region as the higher density requires more time of processing with that method. To increase the effectiveness and accuracy of the calculation, the authors [20] proposed a hybrid solution with both continuum and DSMC-based methods if there is a criterion for the CFD failure.

Pal et al. [22] were able to model a plasma jet using the continuum approach and showed that the NS equations are capable of capturing the flow –thermal structures of the jet. Candler et al. [23] and Erdman et al. [24] also provided studies using the NS equations for the plume, obtaining good results for the emissive properties of the two-phase flow. Both studies concluded that the NS equations were only useful for rough estimations due to the faults they present on rarefied flows.

1.5. Work Description and Objectives

This work aims to study the influence of the aluminium particles on the exhaust plume of the third stage of the VEGA rocket. This analysis shall be done in two separate sets of calculations, to provide a comparison between the effects in a low altitude flight and in a high altitude flight in near vacuum. Several factors are taken into account: altitude (outflow boundary conditions), particle size, particle initial distribution. In order to understand the problem and its implications, the following calculations were done:

- Obtainment of an inviscid flow solution for a one phase gaseous flow of air. This allows a first analysis of the flowfield and how it behaves in high altitudes, especially when it comes to shock waves and numerical behaviour.
- Introduction of the aluminium particles on the initial flow, producing a multiphase flow.
- Analysis and post-processing of the previous solution in order to understand the changes between the initial one phase solution and the multiphase solution.
- Creation of an alternative particle distribution model in order to compare the resulting flow to the ones obtained previously.
- Repetition of the previous flow calculations for the low altitude conditions, providing a comparison of the trajectory changes and plume physical properties between both cases.

The calculations described before allow a good understanding of the interaction between the particles and the flow. To reduce the time consumed and the computational resources used, these calculations were directed in a way that they allow a qualitative analysis to the problem. A quantitative analysis will not be presented since there is not enough data about the particle distribution to guarantee the accuracy of the simulation.

The main goal of this procedure is to provide a preliminary analysis that shows the qualitative effect of the metallic particles used in solid rocket boosters. That is intended to be a starting point for short-plan future works, either on mesh convergence, geometry improvements, or even to compare results from other methods. In a long term project, these results can then be implemented in radiation modelling and combustion analysis.

1.6. Thesis Layout

This thesis is divided in five main sections: introduction, theoretical fundamentals, calculations and discussion of the results, future developments and conclusions.

This chapter is the introductory chapter that explains the objectives and motivation for this work, as well as some insight at the problem studied. The chapter also covers a review of previous studies under several areas of study that will be present in the calculations.

Chapter 2 provides a general overview of the physical and mathematical concepts needed to understand the problem in study, namely nozzle aerodynamics, plume properties and multiphase flows. The theory is based in several books and articles and will also be referred in the discussion sections.

Chapters 3 and 4 present the calculations made during the elaboration of the main part of the work. They present a list of assumptions and simplifications, as well as some details in the computational models used for each case considered. The final part of each section has a brief discussion of the results obtained as well as the conclusions that can be taken from each result.

Chapter 5 lists the most important future developments that should be done to improve this work and the quality of the results. This chapter is one of the most important parts of the thesis as it proposes several possible solutions to the main problems encountered during the calculations, as well as improvements to be done to the computational model. The future developments chapter also addresses the future analyses that make use the results obtained in order to reach a more useful and complete study.

Finally, the last chapter addresses the final conclusions of the entire work, summarizing the discussion written along the solution chapters.

2. PHYSICAL CONSIDERATIONS

2.1. Compressible Flows

Although in real life all fluid flows are compressible, there are some conditions in which it is possible to simplify the flow analysis by assuming the fluid with a constant value for ρ. For a Mach number lower than 0.3 the fluid can almost always be treated as incompressible, otherwise the compressibility effects can't be neglected. Liquid flows and low speed gaseous flows are examples that can be modelled as incompressible with good accuracy.

In gaseous supersonic fluid flows through nozzles, however, this hypothesis is not valid, as there are very high velocities caused by large pressure gradients. These pressure gradients are accompanied by density changes that can't be neglected due to the large compressibility of gases. Therefore, the equations that describe the flow will be presented further.

2.1.1. Flow Regimes

Compressible flows may be split in various flow regimes [25] that are characterised by their Mach number M, defined by equation (1), where U is the fluid velocity and a is the speed of sound defined for a perfect gas by $a = \sqrt{\gamma RT}$.

$$M = \frac{U}{a} \tag{1}$$

Therefore, considering an aerodynamic body in a flowing gas, four main flow regimes can be identified: subsonic flow, transonic flow, supersonic flow and hypersonic flow.

Subsonic Flow **–** $\mathrm{M}_\infty \leq 0.8$

A flow where the Mach number is less to the unity in every point is called a subsonic flow. In this type of flow, the initially straight streamlines deflect once they reach an obstacle, that is, the flow is forewarned of the presence of that object.

Transonic Flow **–** $0.8 \leq \mathrm{M}_\infty \leq 1.2$

A transonic flow is a flow where the Mach number is lower than unity, but that in some regions the flow expansion will lead to a local Mach number higher than 1. This kind of flows is then composed by a supersonic region and a subsonic region, and therefore shock waves may be generated.

***Supersonic Flow* –** $\mathrm{M}_\infty > 1$

A supersonic flow is a flow that has $M > 1$ everywhere. In this case, information can only propagate downstream until it reaches an obstacle like an expansion wave or a shock.. In the shockwave, the streamline deflects discontinuously, producing drastic changes in flow properties. During an expansion, the flow deflects continuously and in an isentropic process.

***Hypersonic Flow* –** $\mathrm{M}_\infty > 5$

Hypersonic flow is a special case of a supersonic flow. As the Mach number increases, the changes provoked by the shockwaves become more and more dramatic and this leads to very high temperatures, causing dissociation and ionization in the gas (like a reacting flow). These changes happen gradually with the increase in Mach number and are very dependent on the flow conditions. However, as a general rule, $M = 5$ is considered as the boundary in which the flow starts to be treated as hypersonic.

2.1.2. Conservation Equations

The principles behind the obtainment of the conservation equations are based on the fundamental laws of nature: conservation of mass, conservation of energy and the second law of Newton. These laws and equations are fundamental to understand the physics behind a compressible fluid flow.

The three basic conservation law equations – continuity, momentum and energy – together with the perfect gas equations provide the tools to analyse and describe a compressible non-reacting flowfield of a gas.

Continuity Equation

The continuity equation [22, 26] describes the physical principle of conservation of mass in its differential form:

$$\frac{\partial \rho}{\partial t} + \nabla \cdot (\rho \mathbf{V}) = 0 \tag{2}$$

Momentum Equation

The momentum equation, also known as equation of motion, describes Newton's second law that states that the time rate of change of momentum of a body equals the net force $\mathbf{F}$ exerted on it [25], written as:

$$\frac{d}{dt}(m\mathbf{V}) = \mathbf{F} \tag{3}$$

The differential form of the momentum equation [22, 26] is given by:

$$\frac{\partial(\rho\mathbf{V})}{\partial t} + \nabla\cdot(\rho\mathbf{V}\mathbf{V}) = -\nabla p + \nabla\cdot\tau_{ij} + \rho\mathbf{f} \tag{4}$$

For a Newtonian fluid, the viscous stress tensor can be written as:

$$\tau_{ij} = \mu\left[\left(\frac{\partial v_j}{\partial x_i} + \frac{\partial v_i}{\partial x_j}\right) - \frac{2}{3}(\nabla\cdot\mathbf{V})\delta_{ij}\right]$$

The replacement of this term in the differential form of the momentum equation – equation (4) – results in the classic Navier-Stokes equation.

Energy Equation

The last of the conservation equations describes the energy conservation principle, also known as the First Law of Thermodynamics, which states that the rate of change of the energy $\dot{E}$ of the fluid must equal the rate of work done on the fluid $\dot{W}$ plus the rate of heat added or subtracted to the fluid from the surroundings $\dot{Q}$ [25]. It can be generally expressed as:

$$\dot{E} = \dot{Q} + \dot{W} \tag{5}$$

The differential formulation of the energy equation [22, 26] is written as:

$$\frac{\partial}{\partial t}\left(\rho\left(h + \frac{V^2}{2}\right)\right) + \nabla\cdot\left(\rho\mathbf{V}\left(h + \frac{V^2}{2}\right)\right) = -\nabla\cdot(k\nabla\mathrm{T}) + \frac{\partial p}{\partial t} + S \tag{6}$$

2.2. Nozzle Theory

The performance of a rocket propulsion system is directly related to the nozzle design. In order to determine several design parameters such as the nozzle size or geometry, there are mathematical tools that can be expressed in the form of thermodynamic relations that describe the processes occurring in the nozzle as the gas expands. These equations describe a theoretical quasi-one-dimensional flow, which is in fact a simplification of the real two or three-dimensional aerothermodynamic flow. Despite this, they can provide adequate and useful results for the analysis of rocket propulsion systems.

The derivation of the quasi-one-dimensional flow theory, used for the nozzle performance studies and aerothermodynamic analysis, is based on the ideal rocket model. This theory follows the following assumptions [1]:

1) The working fluid is a gas and obeys the perfect gas law.
2) The mixture is assumed to be homogeneous.
3) The flow in the nozzle is adiabatic (no heat is transferred across the nozzle walls).
4) The fluid viscosity is not taken into account and boundary layer effects are neglected.
5) There are no shock waves or discontinuities in the nozzle flow.
6) The flow is steady – transient effects can be neglected.
7) At the nozzle trailing edge, the fluid exhaust velocity is directed axially.
8) The flow properties – pressure, temperature, velocity and density – are constant across the section of the nozzle trailing edge.
9) The flow is chemically frozen and no reactions occur in the nozzle.

These assumptions are very accurate and closely describe the real flow in the nozzle. There are errors of 1 to 5% [1] when neglecting the heat losses, the boundary layer and the transient fluctuations, and most of the other assumptions are actually requirements for a good rocket propulsion system, leading to a close modelling of the real conditions. With the ideal rocket, the mathematical expressions can now be developed in order to understand in more detail how the flow behaves in the nozzle.

2.2.1. Thermodynamic Relations

The thermodynamic relations referred before are the result of the application of basic thermodynamic principles, like conservation of energy, to the flow. The resulting expressions will relate the main properties of the gas and will allow a theoretical analysis to what should be happening during the expansion process. There are several concepts that will be summarized: perfect gas law, enthalpy, energy and entropy.

Perfect Gas

By definition, a perfect gas is one in which intermolecular forces are neglected [25]. This approach is widely used in compressible flow applications, since at the temperatures and pressures characteristic of them the molecules are widely separated, providing very small intermolecular forces.

The equation of state for a perfect gas was then derived and can be expressed as:

$$p = \rho RT \tag{7}$$

Equation (7) is defined in terms of mass, and the gas constant has a value of $R = 287\, J/(kg \cdot K)$ for a flow of air. If dealing with moles, then the equation of state will have the following formulation, where n is the number of moles, $\mathcal{V}$ is the volume and $\mathcal{R} = 8314\, J/(kmol \cdot K)$ is the universal gas constant in terms of moles, and is constant for every gas:

$$p\,\mathcal{V} = n\mathcal{R}T$$

Enthalpy

In an equilibrium gas mixture, energy and enthalpy are functions of both the temperature and the volume. However, if the gas is not chemically reacting and we ignore the intermolecular forces, we have a thermally perfect gas, where energy and enthalpy, as well as the specific heats c_v and c_p are functions of the temperature only and are given by:

$$e = e(T) \Rightarrow de = c_v dT \tag{8}$$

$$h = h(T) \Rightarrow dh = c_p dT \tag{9}$$

For a calorically perfect gas, the specific heats are constant, which is a good approximation for several compressible flow applications as long as the temperatures don't get too high. For a supersonic nozzle with temperatures over 1000 K, this assumption leads to a bigger error as the specific heats will vary with the temperature.

The specific heats are related to each other through the gas constant R and the specific heat ratio γ according to the following expressions:

$$c_p - c_v = R \tag{10}$$

$$\gamma = \frac{c_p}{c_v} \tag{11}$$

2.2.2. Quasi-One-Dimensional Flow

To analyse the flow inside the nozzle it is better to simplify the conservation equations described earlier before applying them to the nozzle flow. It can be assumed then, that the flow properties are uniform across any section of the flow $-p = p(x)$, $\rho = \rho(x)$, $\mathrm{V} = u =$

$u(x)$ and $A = A(x)$ – , and that the flow is steady and adiabatic. Such a flow is called a quasi-one-dimensional-flow.

The equations that rule quasi-one-dimensional flows are obtained from the basic conservation equations described before, when applied to a control volume inside the nozzle (Figure 5). Let's consider the subscript 1 as the control volume inlet and the subscript 2 as the control volume exit. The integral form of the continuity equation integrated over the control volume, leads to:

$$\rho_1 u_1 A_1 = \rho_2 u_2 A_2 \tag{12}$$

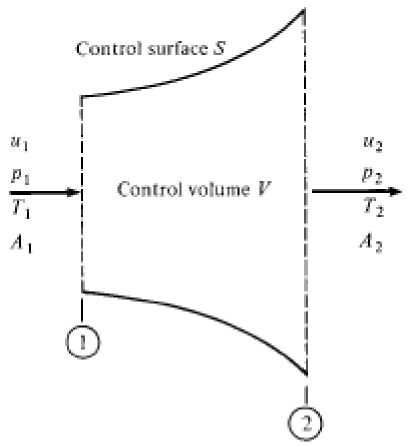

Figure 5 – Finite control volume for quasi-one-dimensional flow [25].

Each term correspond to the surface integral over sections 1 and 2 respectively. The surface integral along the nozzle wall is zero, since the wall is considered to be a streamline.

The momentum equation for a steady quasi-one–dimensional flow results from the application of its integral form to the control volume shown before and it leads to:

$$p_1 A_1 + \rho_1 u_1^2 A_1 + \int_{A_1}^{A_2} p \, dA = p_2 A_2 + \rho_2 u_2^2 A_2 \tag{13}$$

The extra integral that appears in this equation represents the pressure forces on the nozzle walls between sections 1 and 2.

Finally, the energy equation leads to:

$$h_1 + \frac{u_1^2}{2} = h_2 + \frac{u_2^2}{2} \tag{14}$$

This equation is particularly important as it shows that the stagnation enthalpy defined as $h_0 = h + u^2/2$ is constant along the flow under the conditions described before.

The continuity equation can also be written in its differential form. For a steady, adiabatic, quasi-one-dimensional flow, from equation (12):

$$d(\rho u A) = 0 \Rightarrow \frac{d\rho}{\rho} + \frac{dA}{A} + \frac{du}{u} = 0$$

Manipulating this expression and adding the relationship between the density change and the velocity change (caused by the pressure variation) $d\rho/\rho = -M^2\, du/u$, we obtain a very useful relation between area changes and velocity. This relation may be summarized with the following equation [25]:

$$\frac{dA}{A} = (M^2 - 1)\frac{du}{u} \tag{15}$$

The equation above is often called the area-velocity relation. It is now clear that in the subsonic part of the nozzle ($M < 1$), a decrease in the cross sectional area causes an increase in the velocity. In the supersonic region ($M > 1$ – after the throat), on the other hand, an increase in area will also make the velocity increase. It is expected then, that in a convergent-divergent nozzle that has subsonic flow at the inlet and sonic conditions at the throat, the velocity will always rise in the direction of the flow.

2.2.3. Isentropic Relations

For an isentropic flow, the following relations provide a useful way to find the pressure, temperature and density along the nozzle, based on the Mach number of the flow. These are called the isentropic relations, and relate the stagnation properties with the static properties.

$$\frac{T_0}{T} = 1 + \frac{\gamma - 1}{2} M^2 \tag{16}$$

$$\frac{p_0}{p} = \left(1 + \frac{\gamma - 1}{2} M^2\right)^{\frac{\gamma}{\gamma - 1}} \tag{17}$$

$$\frac{\rho_0}{\rho} = \left(1 + \frac{\gamma - 1}{2} M^2\right)^{\frac{1}{\gamma - 1}} \tag{18}$$

Although the stagnation temperature, as the enthalpy, remains constant as long as the flow is adiabatic, the same is not true for the stagnation pressure, as it needs the flow to be isentropic in order to be kept constant [1].

2.2.4. Rocket Performance Parameters

2.2.4.1. Area Ratio

The area ratio is defined by the ratio between the areas of two sections of the nozzle and can be derived from the relations described before.

$$\frac{A_2}{A_1} = \frac{M_1}{M_2}\sqrt{\left\{\frac{1 + [(\gamma - 1)/2]M_2^2}{1 + [(\gamma - 1)/2]M_1^2}\right\}^{(\gamma+1)/(\gamma-1)}} \tag{19}$$

This ratio depends much on the flow desired Mach number and the flow specific heat ratio γ. In a more practical way, the nozzle expansion ratio is seen as the ratio between the nozzle exit area and the throat area A_e/A_t, providing a very useful design parameter.

2.2.4.2. Exhaust Velocity

When going through a converging-diverging nozzle, the flow's thermal energy is converted in kinetic energy. This corresponds to a decrease in temperature and pressure and an increase in velocity. Therefore, velocity can reach very large values in the nozzle exit, depending on the expansion ratio and on the chamber and ambient conditions.

For a general rocket, the exit velocity can be obtained from equation (14) and is defined by:

$$v_e = \sqrt{2(h_i - h_e) + v_i^2} \tag{20}$$

For a chamber section much larger compared to the nozzle throat, we may assume that the inlet velocity is zero and that the inlet temperature is given by the chamber temperature (which is equal to the stagnation temperature since the velocity is zero). Rewriting equation (20) we obtain a relationship between the exit velocity and the inlet temperature, the pressure ratio and the gas properties:

$$v_e = \sqrt{\frac{2\gamma}{\gamma - 1}RT_0\left[1 - \left(\frac{p_e}{p_i}\right)^{(\gamma-1)/\gamma}\right]} \tag{21}$$

From this expression we can also obtain a value for the maximum theoretical velocity, which is reached for an infinite expansion to vacuum under optimum conditions ($p_e = p_a = 0$):

$$v_e = \sqrt{\frac{2\gamma}{\gamma - 1}RT_0} \tag{22}$$

This value corresponds to the thermal energy content of the fluid, when it is all transferred to kinetic energy. Although we are talking about an infinite expansion, the exit velocity is finite because it is limited by the thermal energy, which is not infinite.

2.2.4.3. Thrust and Specific Impulse

The net thrust F produced by the rocket is the result of the reaction force on the nozzle structure caused by the momentum of the flow. It can be derived from a balance of momentum to the nozzle and is given by:

$$F = \int (\rho V \cdot dA) \cdot V + \int p \, dA \tag{23}$$

$$F = \dot{m} v_e + (p_e - p_a) A_e \tag{24}$$

Equation (24) assumes constant properties at the inlet and at the outlet, which is not true for a three-dimensional flow. It also assumes a control volume surrounding the entire rocket. Despite this, it is a simple but good approximation for the thrust generated by a rocket.

Equation (24) can also be written in terms of the known properties at the nozzle inlet, throat and exit, and a thrust coefficient C_F can be found.

$$F = A_t p_i \sqrt{\frac{2\gamma^2}{\gamma - 1} \left(\frac{2}{\gamma + 1}\right)^{(\gamma+1)/(\gamma-1)} \left[1 - \left(\frac{p_e}{p_i}\right)^{(\gamma-1)/\gamma}\right]} + (p_e - p_a) A_e = C_F A_t p_i \tag{25}$$

The thrust coefficient hits a maximum for optimum expansion conditions. This value is an important parameter for nozzle design considerations as it provides a maximum for the thrust.

The specific impulse can be described as the thrust generated per unit mass of propellant. Considering a constant thrust and propellant burning rate, we have:

$$I_{sp} = \frac{F}{g\dot{m}} = \frac{V_{eff}}{g} \tag{26}$$

where g is the gravitational acceleration constant and V_{eff} is the effective exhaust velocity given by:

$$V_{eff} = \frac{v_e + (p_e - p_a) A_e}{\dot{m}} \tag{27}$$

The specific impulse is another useful parameter for nozzle design as it doesn't depend on the propellant consumption rate and will depend only on the nozzle performance itself.

2.3. Two-Phase Flow: Forces Acting on the Particles

The coupling between the gaseous flow and the solid particles is made through energy and momentum balances to the system, measuring the exchanges between both phases.

While inserted in the flow going through the nozzle, the particles' trajectories are influenced by the viscous forces and pressure forces exerted on them by the surrounding flow field. In order to quantify their influence, let's apply a force balance to the particle, equalling the particle acceleration to the force per unit mass, as suggested by the second law of Newton. Therefore, the particle acceleration per unit mass is given by the sum of drag forces $\mathbf{F}_D$, pressure forces $\mathbf{F}_P$, the gravitational force $\mathbf{F}_G$ and additional forces $\mathbf{F}_X$ like the "virtual mass" force and the thermophoretic force.

$$\frac{\partial \mathbf{V}_p}{\partial t} = \mathbf{F}_D + \mathbf{F}_P + \mathbf{F}_X + \mathbf{F}_G \tag{28}$$

In this analysis the additional forces and the gravity force will be neglected as they do not contribute as much as the other two components.

The drag force per unit mass is given by

$$\frac{\mathbf{F}_D}{m_p} = \frac{1}{2}\rho_f S C_D \left(\mathbf{V}_f - \mathbf{V}_p\right)^2 \tag{29}$$

where the subscript f refers to the fluid and the subscript p refers to the particle.

The drag coefficient C_D can be obtained through Morsi and Alexander's experimental correlation for the drag on spherical particles [27]:

$$C_D = a_1 + \frac{a_2}{Re} + \frac{a_3}{Re^2} \tag{30}$$

The coefficients a_1, a_2 and a_3 are available in the original article and depend on the range of Reynolds numbers considered. The Reynolds number for this correlation is based on the particle diameter and is given by:

$$Re = \frac{\rho_f d_p \left|\mathbf{V}_p - \mathbf{V}_f\right|}{\mu_f} \tag{31}$$

The pressure forces are originated by the pressure gradient that exists when the flow compresses or expands. The total pressure force per unit mass exerted on a particle is then given by the following equation:

$$\frac{\mathbf{F}_P}{m_p} = -\int \frac{\nabla p \, d\mathcal{V}_p}{m_p} = \frac{-\nabla p}{\rho_p} \tag{32}$$

From the conservation of momentum law applied to the control volume containing the particle the pressure gradient may be written in terms of the fluid velocity gradient.

$$-\nabla p = \rho_f \mathbf{V}_{f0} (\nabla \cdot \mathbf{V}_f)$$

As the initial instantaneous fluid velocity $\mathbf{V}_{f0}$ is the same as the particle velocity which is constant in all the control volume, $\mathbf{V}_p = \mathbf{V}_{f0}$, and thus:

$$\frac{\mathbf{F}_P}{m_p} = \frac{\rho_f}{\rho_p}\mathbf{V}_p(\nabla \cdot \mathbf{V}_f) \tag{33}$$

As it can be seen from the previous expression, if $\rho_p \gg \rho_f$ then the pressure forces are negligible and the particle motion is governed by the drag force [27] [28].

2.4. Characteristics of Exhaust Plumes

The properties of the exhaust plume of a rocket can be of great importance in a space mission. Radiation form the plume to the payload as well as to other sensitive surfaces is an important consideration. Since this is dominated by the radiation from the alumina in the plume, the ability to predict the physical behaviour of rocket hot plumes is of key importance to mission designers.

2.4.1. Nozzle Expansion Process

The expansion process inside the nozzle is controlled by the pressure at the nozzle exit and by its expansion ratio. As shown before, an ideal nozzle that maximizes performance should have an exit pressure equal to the ambient pressure. In reality, this optimum condition doesn't happen even at the design altitude, and two different situations occur.

If the exit pressure is greater than the ambient pressure, the flow is underexpanded and will automatically expand once it leaves the nozzle, until it reaches the pressure outside. The additional expansion isn't providing any thrust since it happens outside of the nozzle, leading to a loss of efficiency when compared to the optimum solution.

On the other hand, if the ambient pressure is greater than the pressure at the nozzle exit, it means that the nozzle expansion ratio is too big and the flow is overexpanded. The exhaust stream contracts and leads to a loss of thrust (from the ideal case) due to the negative pressure difference, as can be seen in equation (24). If the exit pressure is much lower than the ambient pressure, then there is a chance of having the flow separating from the nozzle wall, reducing even more the nozzle performance.

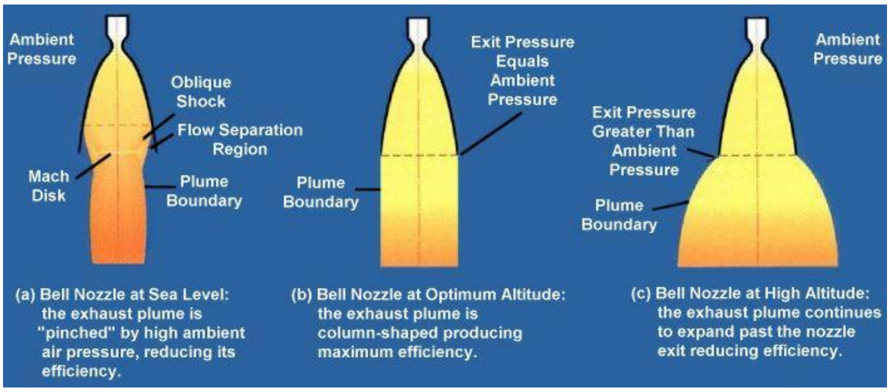

Figure 6 – Difference in flow behaviour between (a) overexpansion, (b) ideal expansion and (c) underexpansion. (Image credit to Aerospaceweb.org)

Due to the variation of pressure with altitude, it is expected that the nozzles go through several operating conditions. Therefore, the choice of the design altitude is crucial to maximize the rocket performance. Usually, the use of several stages allows the avoiding the overexpanded situation which would lead to the worst situation possible of thrust loss. On take-off, it is imperative to prevent that. At higher altitudes it is expectable that the flow is underexpanded, since the rockets are operating at widely ranging altitudes that differ from the design altitude.

During ground level testing, nozzles that are destined to higher altitude operation show an overexpanded flow, but they still allow the extraction of several data related to the flow characteristics that can then be applied to the plume analysis in high altitude conditions.

2.4.2. Exhaust Plumes

A rocket exhaust plume is formed by the expansion of the combustion products inside the chamber. These reach high velocities at the nozzle exit, consequence of the conversion of thermal to kinetic energy. Although the plume temperature is lower than the combustion temperature, it usually is still high enough to cause a worry about the emission of thermal radiation.

In the plume two main regions can be defined. The inviscid core, an almost inviscid region that is surrounded by a viscous layer, where the plume gases mix with the atmosphere, called the mixing layer.

In the core of an underexpanded gaseous plume the flow will be forced to turn by the dynamic pressure of the outflow. This is made through a shock wave called the intercepting shock that propagates until it reaches the axis of the plume. Here, the shock reflects and compresses the gas above the external pressure. This leads to a new shock that creates a pattern of Mach diamonds (like shown in Figure 7). The flow within the intercepting shocks is called the intrinsic core.

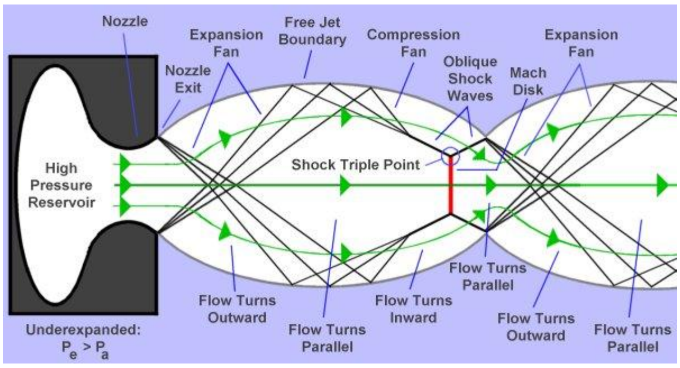

Figure 7 – Wave structures that create shock diamonds in an underexpanded flow.
Image credit to Aerospaceweb.org

Figure 8 – Mach diamonds during a NASA firing test.
Image credit to Mike Massee/XCOR Aerospace and NASA.

As the altitude increases, the shocks get stronger and the dissipative effects start to rise, eliminating the periodic structure of the diamonds. At high altitudes, it is common that only the first cell of the intrinsic core is evident.

The mixing layer is the viscous layer that mixes with the surrounding atmosphere. In this region, momentum and energy are exchanged and chemical reactions occur. If the rocket velocity is less than the exhaust velocity, a drag effect comes in and leads to a reconversion of kinetic energy in thermal energy, thus increasing the temperature.

In high altitude supersonic rockets, two shock waves are formed: one ahead of the plume and another one in the nose of the rocket. For high-diameter plumes, the latter will detach and will also appear ahead of the plume, like is shown in Figure 9.

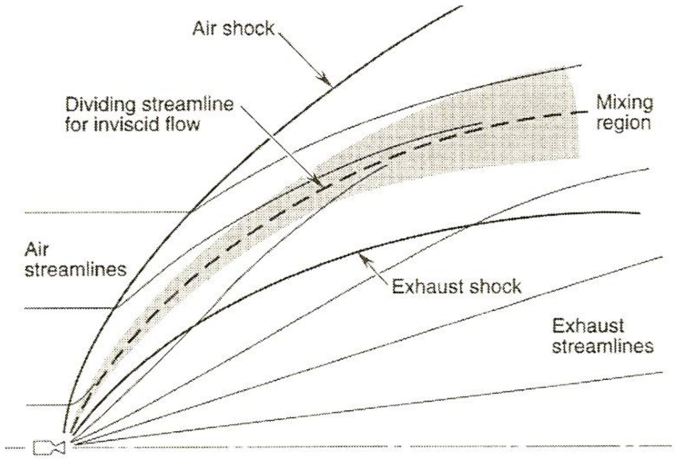

Figure 9 – Structure of high altitude plumes.

Image credit to [29]**.**

2.5. Two-Phase Flow Plumes

Solid propellants usually create products in a condensed liquid or solid phase that will appear in the plume. Although the overall plume structure doesn't change much with the particles if they are small sized, some larger particles can change the plume significantly.

Aluminium oxide, or alumina (Al_2O_3), is a common product of solid propellant combustion, since aluminium is introduced to improve performance and combustion stability. The combustion process of a liquid aluminium drop originates a bimodal distribution in sizes, constituted by two types of particles: agglomerate and smoke. Agglomerate is the oxide that is formed attached to the aluminium liquid particle, while the smoke is formed by very small particles of oxide that detach from the agglomerate. Despite this, it is common to neglect the smoke when modelling the flow, since the shear forces in the nozzle often force the small particles to reattach to the bigger ones. Therefore, the particle size distribution is more representative of agglomerate sizes than smoke. The particles are almost spherical in shape due to them being formed as a liquid, and their size depends on several factors, like the combustion itself, the nozzle expansion ratio, the nozzle throat diameter and the Weber number (during the liquid phase).

During the plume expansion, alumina particles will follow the flow up to a certain angle that is determined by the particle size. Therefore, the solid particles will create a conical core, composed by bigger particles in the middle and smaller particles on the periphery, that won't be as open as the gaseous plume, and allows a separation region to be observable. The plume velocity will also be lower in the solid core region, as the particles will decelerate the gaseous flow.

2.6. Rarefied Flows Considerations

In high altitude plumes, the outside pressure is too low and the flow starts getting rarefied. Rarefied gases have a large space between each molecule and must be addressed not as a continuum media but as a group of discrete particles interacting and colliding with each other. In order to help defining the various flow regimes under rarefied conditions, they are divided into four categories based on a dimensionless number named after the Danish physicist Martin Knudsen (1871-1949). The Knudsen number Kn is a measure of the rarefaction of the gas and is defined as the ratio of the mean free path, λ, (mean distance between the molecules) and a characteristic length, L.

$$Kn = \frac{\lambda}{L} \tag{34}$$

This number may also be related to the Mach number and the Reynolds number of the flow by the following relation [30]:

$$Kn = \frac{M}{Re}\sqrt{\frac{\pi\gamma}{2}} \tag{35}$$

This expression allows a more physical understanding of the physical influence of the Knudsen number.

Continuum flow	Kn < 0.001
Slip flow	0.001 < Kn < 0.1
Transition flow	0.1 < Kn < 10
Free molecular flow	Kn > 10

Table 2 – Flow categories based on the Knudsen number.

Table 2 shows the classification of the flow regimes based on the Knudsen number. There are four main regimes that can be defined as [31]:

- **Continuum flow –** described very well by the Navier-Stokes equations.
- **Slip flow –** this regime is still accurately described by the Navier-Stokes equations, however, it needs an adaptation on the velocity and temperature boundary conditions.
- **Transition flow –** here the Navier-Stokes equations start to fail and the Boltzmann equation becomes a better way to describe the flow behaviour.
- **Free molecular flow –** there are almost no collisions between the molecules and the flow is dominated by wall/particle interactions.

3. HIGH ALTITUDE PLUME

This chapter focus on the CFD calculations for a high-altitude solid rocket plume using the commercial software FLUENT®. These calculations aim to verify the plume behaviour at high-altitudes, where the ambient pressure is near vacuum and they will allow the obtainment of the particle-affected region, as well as the influence of those particles in the original single phase plume. The code used allows the introduction of the particles by a discrete phase Langrangean method, leading to the two-phase flow solution. These calculations are performed under several different particle initial conditions, in order to vary their size and distribution, which allows the verification of the influence of these parameters on the plume final temperature distribution and therefore in the radiation emitted by it. It is important to notice that the calculations done in this chapter only present a qualitative analysis and they are not representative of the correct values of any fluid or particle property.

3.1. Single-Phase Flow Solution

3.1.1. Assumptions

For a first step, in order to reduce the computational effort and to allow an easier analysis of the results, the following assumptions were used to simplify the problem:

- Internal and external fluids are modelled as air, assuming ideal gas conditions.
- The flow is calorically perfect (constant specific heats).
- The operating pressure was set to zero. The operating pressure is the difference between the gauge pressure and the absolute pressure [26].
- The flow is chemically frozen.
- The flow is modelled as a continuum, since the computational software used does not allow a rarefied approach. Besides, when looking at previous studies [20] [21] [22] [23] [24], continuum approximations on the plume are found to provide consistent results, especially in the core. This will be taken into account when analysing the results.
- The boundary layer in the nozzle wall has small influence in the resulting flow.
- Turbulence models were not included in order to save computational time. Further analysis is required.
- Steady flow was assumed.
- Ionization and dissociation were neglected although they are present in a hypersonic flow.

The problem was modelled as a 2D axisymmetric problem.

3.1.2. Viscosity Model

The dynamic viscosity of the air is a function of the temperature. Therefore the laminar viscosity value was defined according to the three-coefficient Sutherland law, given by the following expression [26] [32]:

$$\mu = \mu_0 \left(\frac{T}{T_0}\right)^{3/2} \frac{T_0 + S}{T + S} \tag{36}$$

The coefficient μ_0 is the reference viscosity (evaluated at the reference temperature T_0) and S is the Sutherland constant. The correspondent values for air can be found in the literature (ref. [32]) and are also listed here:

- $\mu_0 = 1.716 \times 10^{-5}\ kg/(ms)$
- $T_0 = 273.15\ K$
- $S = 110.4\ K$

The Sutherland law is based on the kinetic theory of the ideal gases and it provides a relationship between the dynamic viscosity of an ideal gas and its absolute temperature. This formula has given accurate results and it’s commonly used to model ideal gas viscosities.

3.1.3. Boundary Conditions

Gas properties (Air):

- $c_p = 1006.43\ J/(kg \cdot K)$
- $k = 0.0242\ W/(m \cdot K)$
- Molar mass - $M = 28.966\ kg/kmol$

The combustion chamber and the outflow properties were provided by ESA.

Combustion chamber:

- $T_0 = 3401\ K$ (expected temperature in the chamber after the combustion)
- $p_0 = 74\ bar$

The velocity inside the chamber is very small. Therefore, these conditions correspond to the flow stagnation properties.

Nozzle wall:

- Slip wall with no shear stress.

The slip wall condition guarantees that no boundary layers will be taken into account in the viscous calculation.

Outflow and ambient conditions:

- $T = 191\ K$
- $p = 0.03\ Pa$
- Supersonic Mach number → $M = 2$

3.1.4. Computational Model

The CFD simulation was made recurring to the commercial code FLUENT®. Previous studies [20] [22] obtained satisfactory results for plasma jets expansion using continuum models using the same code. Equations (2) (4) and (6) are solved together with the state equation of perfect gases and applied to a steady state calculation, eliminating the time dependent terms and simplifying the equations.

The spatial and temporal discretization schemes were chosen to minimize the computational time and resources used by the calculations, in exchange for less quality in the solution. However, as the objective was to get only a qualitatively correct solution, a first-order upwind numerical scheme was used for spatial discretization.

The computational analysis of high-velocity compressible flows is usually done through a density-based or coupled solver [26]. In this solver, the continuity, momentum and energy equations, are solved together. This makes the coupled approach far more robust than the uncoupled approach. However, this also leads to an increase of computational resources needed and to a bigger time of processing. This method was originally developed to solve this specific kind of flowfield where shockwaves and huge pressure and density gradients take place, and it produces a more accurate solution to the problem in study. Because the governing equations are non-linear and coupled, it needs several iterations in order to obtain a converged solution. Therefore, all the calculations presented in this report were obtained with FLUENT's density-based or coupled solver as it is arguably the best option to solve the flowfield in study.

The following chart summarizes the iteration process step by step [26], which is outlined below:

- Update the fluid properties based on the previous iteration or on the initial solution.
- Solve the continuity, momentum and energy equations simultaneously.
- Solve scalar equations such as turbulence and radiation (not used in this calculation).
- Check for convergence.

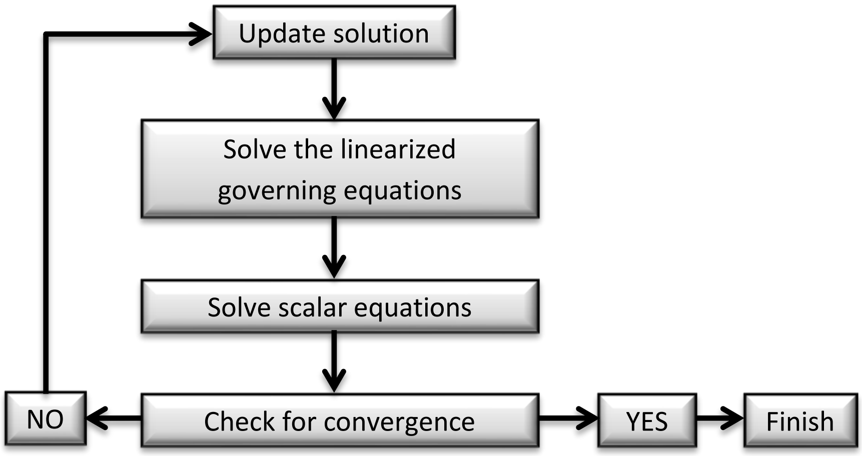

Figure 10 – Overview of one iteration using FLUENT™ density-based solver.

3.1.5. Geometry and Mesh

The geometry and the mesh used for these computations were provided by Dr. Henry Wong from ESA/AOES [33] and are shown below. The mesh used corresponds to the upper half of what is shown in Figure 15 and it was built as a 2D axisymmetric mesh.

The origin of the axes is located in the middle of the left boundary of the combustion chamber, and these axes will be used throughout the whole work.

The nozzle throat is located at about 2.08 meters from the chamber with a diameter of 14.5 cm, and the nozzle length is 4 meters. The nozzle exit diameter is approximately 1 meter. The mesh was refined inside the nozzle and the chamber, as well as along the symmetry axis to capture the shock and expansion waves that will be formed. The following figures show the computational domain and the mesh details at several different locations.

Nozzle

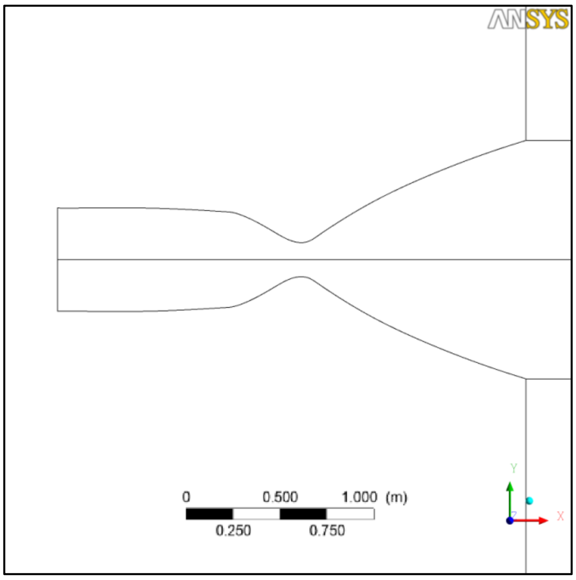

Figure 11 – Nozzle geometry.

Domain

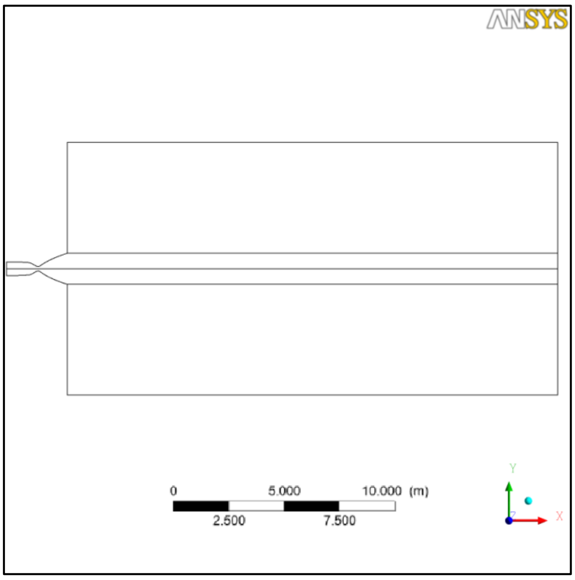

Figure 12 – Computational Domain

Throat Mesh

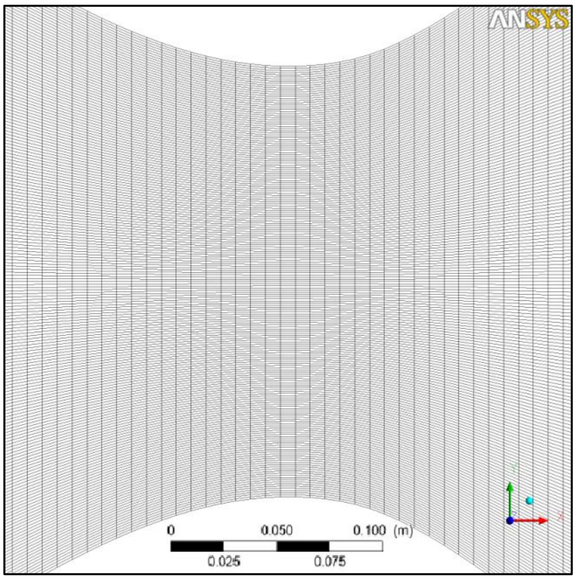

Figure 13 – Detail of the throat meshing.

Nozzle Mesh

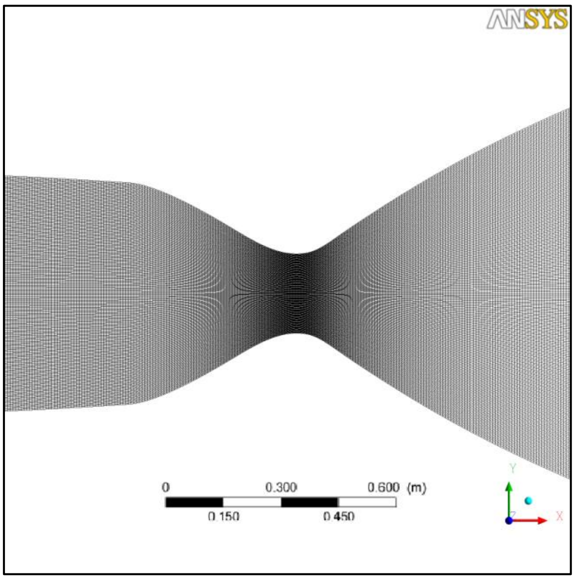

Figure 14 – Zoom of the throat and chamber mesh.

Full Mesh

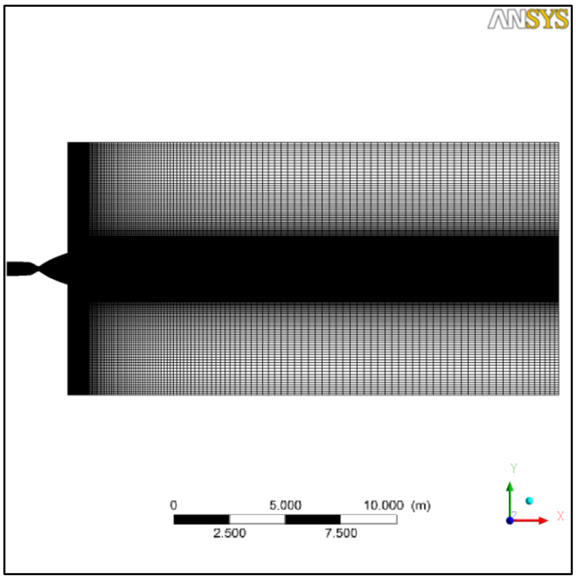

Figure 15 – Grid of the entire domain.

Although the mesh presented before is already refined, in order to check the effect of the mesh on the results two new meshes were analysed. These meshes were obtained by refinement of the entire nozzle and the centreline area, in order to detect the large gradients that occur here, as well as the shock and expansion waves present in the flow.

Number of Elements	Velocity (m/s)	Pressure (Pa)	Temperature (K)	Mach Number
72964	2415.69	7920.22	501.178	5.46049
111163	2416.2	7937.86	499.986	5.46886
384337	2423.02	7905.89	483.613	5.57649

Table 3 – Variation of the flow properties at the nozzle exit with the number of elements.

The previous table show the variation of the mass-averaged properties at the nozzle exit with the number of elements. As it can be observed, there is a very small variation on these values, never going above 3%. Therefore, the original mesh is still preferred, since the increase in computation time makes it a waste of computational resources. The final calculation will include the calculation of the particle trajectories at each set of iterations harshly increasing the processing time, making the mesh choice an important parameter in order to obtain the results needed in the available time. More refined meshes were then verified to be ineffective time wise.

3.1.6. Results

The following figures and charts represent the most relevant results for the high altitude gaseous plume.

Mach Number

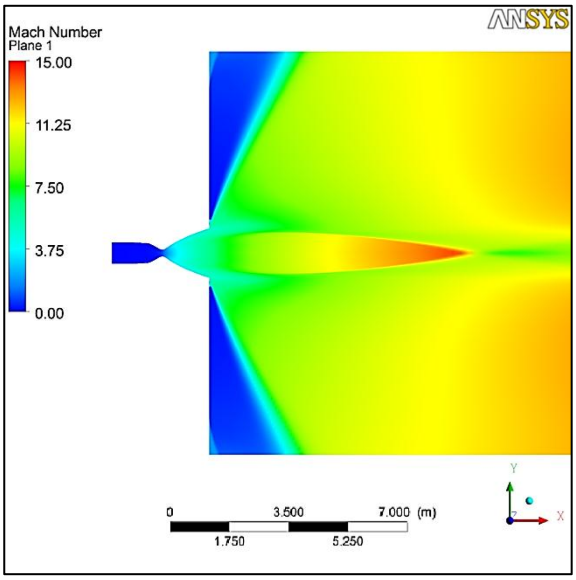

Figure 16 – Mach number contour.

Temperature

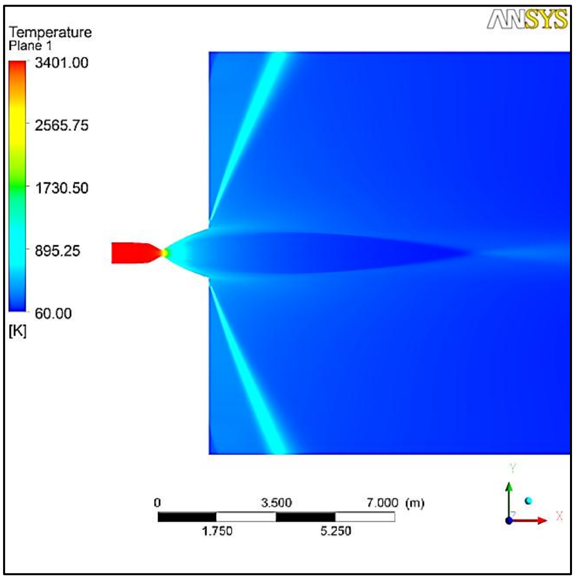

Figure 17 – Temperature contour.

Figure 16 and Figure 17 respectively show the Mach number contours and the temperature contours of the plume. It can be noticed that the Mach number increases to very high values due to the expansion process. The increase in velocity is accompanied by a decrease in temperature, corresponding to the conversion of thermal energy into kinetic energy.

The high temperature band that comes out of the nozzle corresponds to the intersection between the exhaust plume and the external flow. As the external flow is cooler and slower than the flow coming out of the nozzle, an expansion wave is observed in that intersection. If the expansion is considered to be isentropic, then the ratio between the static and total temperatures increases with the Mach number. Due to the energy transferred from the plume to the outflow, in that particular region the total temperature of the outflow rises (see Figure 18). Therefore, in order to keep the T/T_0 ratio, the static temperature will increase to compensate for the increase in total temperature, causing a higher temperature band in the expansion region.

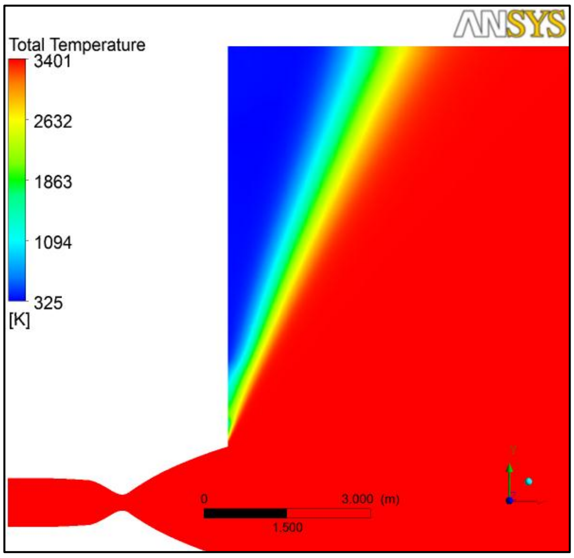

Figure 18 – Total temperature plot.

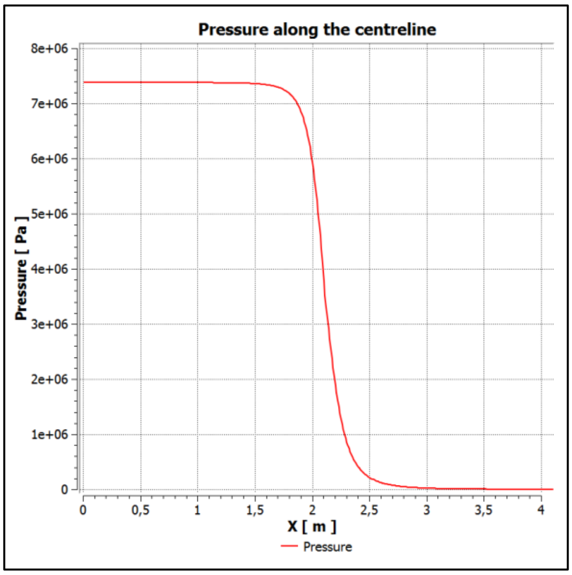

Chart 1 – Pressure along the nozzle centreline.

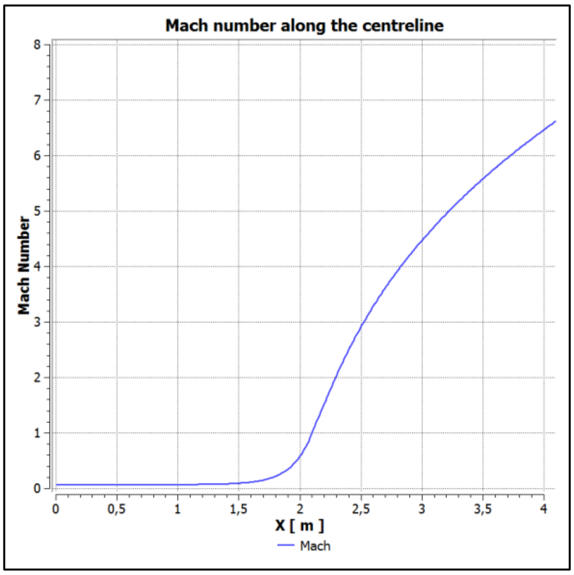

Chart 2 – Mach number along the nozzle centreline.

Chart 1 and Chart 2 show the evolution of pressure and Mach number along the nozzle centreline. According to the general literature for nozzle expansion [25], the pressure is expected to drop harshly on the throat, hitting the critical value at Mach 1. The Mach number develops as expected, increasing both on the divergent and on the convergent part of the nozzle.

Next, two charts are presented (3 and 4) plotting velocity and pressure at the nozzle exit. These results will allow for an estimation of the nozzle performance based on the equations introduced on chapter 2. It can be seen that the properties are not uniform along the section and in order to quantify them a mass average will be used.

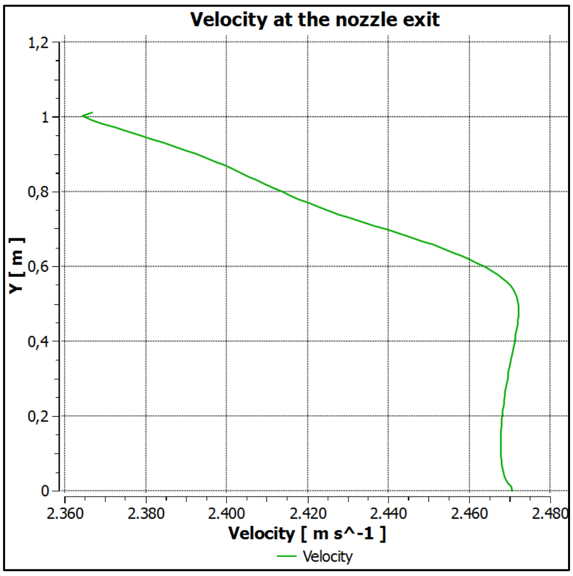

Chart 3 – Velocity at the nozzle exit.

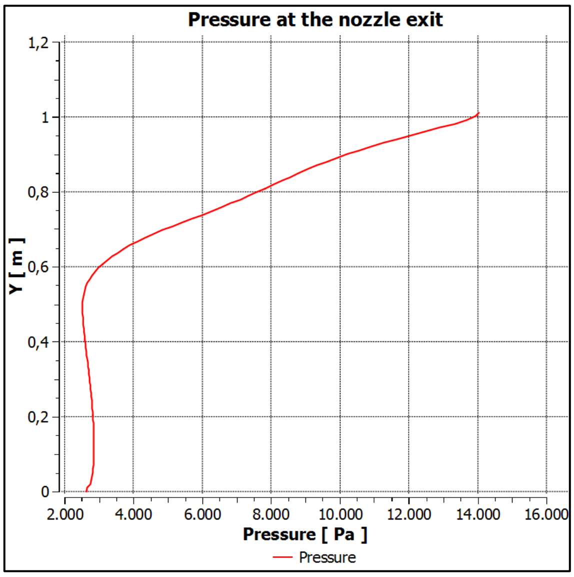

Chart 4 – Pressure at the nozzle exit.

3.1.7. Discussion

Simplifications

The results obtained in this calculation were subject of several approximations that allowed the problem to become simpler and faster to solve. From the points listed at the beginning of this chapter, the approximation related to the hypersonic flow effects is one of the most significant. As the gas expanding in the nozzle has high temperatures and velocities, reaching hypersonic Mach numbers, ionization and dissociation are two important and ever-present phenomena, and neglecting them comes with a reduction of the result accuracy since the models used in the computations are only accurate for non-reacting flows. The molecules of H2O, CO2 and other combustion products will start to dissociate and ionize, meaning that the molecular structure of the compounds is broken and even the electrons may break free from the atoms. In addition to this, due to the increasing vibrational movement of the gaseous molecules, the specific heats of the gas starts depending even more on the temperature and the pressure, which means that the approximation used for these calculations will also provide an error in the results. The high temperatures that are found inside the nozzle can also trigger some additional chemical reactions between the products of the main reactions. In the external plume, there are also afterburning reactions taking place between the exhaust gases and the external air flow in the mixing layer. These reactions and their effect in plume temperature were not considered due to the difficulty on modelling the reactions and the time it consumed.

The ionization and the chemical reactions occurring in the flow turn it into an electrically charged plasma that has several different properties than non-reacting gas flows. Despite this, as seen in previous studies, especially in the work from Subrata et al. [22], the CFD models from FLUENT allow a satisfactory use of the gaseous approximation to model electrically charged plasmas. This way, it is expected that this approximation will still lead to physically correct results.

The other main simplification that was made was the continuum approach used for modelling the flow. As explained before, the Navier-Stokes equations that were solved are valid only for continuum flows. Otherwise, other methods like the DSMC should be used to provide physically correct results. In order to verify the order of magnitude of the errors coming from this approximation, a plot of the flow Knudsen number is shown in Figure 19.

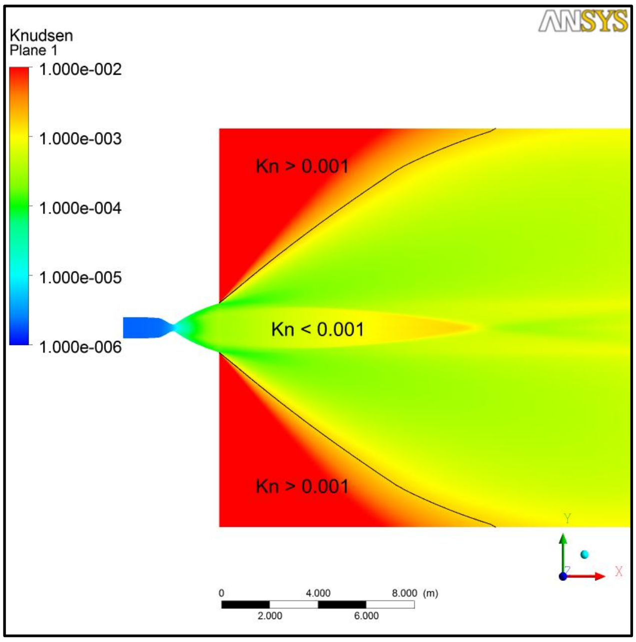

Figure 19 – Knudsen number contour.

Considering the continuum regime to correspond to a Knudsen number lower than 0.001 and according to the plot, it is seen that the continuum model is a valid approach on most of the one-phase gaseous plume core. On the other hand, the higher Knudsen numbers that appear on the mixing layer can lead to numerical errors and to physically wrong results. Although these effects are important to consider, they happen in the most external regions of the plume that are outside of the particle affected area, as will be seen in the next sections. Despite the possible errors, several studies confirm that the continuum model is still reasonable to model these kinds of plumes as shown by Subrata et al. [22] and Selezneva et al. [20].

Results

The flowfield presented in Figures 14 and 15 can be divided in two main regions: nozzle and plume. Since the flow is adiabatic (no heat transfer between the fluid and the nozzle walls and other external sources), the total temperature and total enthalpy remain constant throughout the fluid that comes out of the nozzle. Total pressure is expected to drop due to the dissipative effects from the viscosity. Observing Figure 16, shock and expansion waves come out from the nozzle exit, creating the diamond pattern that is expectable on nozzle plumes. The plots also show that there is a significant part of thermal energy that is converted to kinetic energy during the whole expansion process.

Taking a more detailed look into the nozzle itself, there are some small calculations that can be done to verify the qualitative accuracy of the results. In theory, critical pressure (pressure under sonic conditions) is obtained at $0.528p_0$, corresponding to a value of $3.91 \times 10^6\ Pa$. Considering the pressure variation along the nozzle centreline, plotted in Chart 1, it is observed that this value corresponds to the throat region (around 2.08 meters), as expected. Plots of the pressure and Mach number variations inside a convergent-divergent nozzle are found on several references [25] and show a close resemblance with the charts obtained before.

In order to quantify the influence of the particles in the flow, let's estimate the thrust produced by the rocket. The total thrust will be estimated based on the stream thrust averaging technique given by equation (23) from section 2.2.

Let's consider a control volume around the diverging part of the nozzle, with the inlet at the throat and the outlet at the nozzle exit. This way, the net force that is being exerted on the nozzle walls equals the difference between the force at the outlet and the force at the inlet. Performing the integration at the throat and at the nozzle exit we obtain:

$$F_{throat} = 609\ KN$$

$$F_{exit} = 792.6\ KN$$

$$\boldsymbol{F_{net} = 183.6\ KN}$$

The exhaust Mach number can also be estimated and compared to the numerical solution obtained. It should only be function of the area ratio and a theoretical value can be obtained from equation (19). As the Mach number varies along the section, a mass averaging technique was used to estimate the mean value to compare. It is shown that the mass averaged Mach number obtained has a 7% deviation from the theoretical average value, which is most likely caused by the simplifications assumed in the theoretical formulation for an ideal rocket. It is however safe to tell that the flowfield solution obtained is shown to provide adequate results qualitatively and even quantitatively to some extent. These results will act as the “reference” conditions when checking for the particle effects and will be referred again in the next sections.

Exhaust Mach Number		
Equation (19)	**Numerical Solution**	**Deviation**
5.873	5.460	7.0 %

Table 4 – Comparison between the theoretical exhaust Mach and the value obtained.

3.2. Two-Phase Flow Solution

The two-phase flow was modelled using the previous flow solution and a discrete phase model for the particles. Since the experimental data about the size and the distribution of the particles is very limited, several cases were analysed in order to check the effect of those distributions on the plume behaviour. Two main factors were changed: particle size and particle size distribution.

3.2.1. Assumptions

All the calculations with the particles follow the same assumptions as before for the gaseous flow. The same geometry and boundaries were used.

For the introduction of the particles several additional assumptions were considered:

- The particles are spherical, solid and made of pure aluminium throughout the whole flowfield.
- No oxidation or other chemical reactions take place on the particles.
- No phase change occurs.
- The particles don’t exchange mass with the fluid.
- The volume fraction of the solid particles is small. This assumption is needed to guarantee a good solution from the discrete phase model.

- The forces acting on the particles are only caused by the pressure gradients and by the viscous drag. No other forces were considered.

The modelling of the chemistry and the phase change, although it is possible, would take a much higher time of processing, being too complex to be part of this work.

3.2.2. Particle Information

As stated before, the particles are spherical and constituted by aluminium with the following properties:

- $\rho = 2719\, Kg/m^3$
- $C_p = 871\, J/(Kg \cdot K)$
- $k = 202.4\, W/(m \cdot K)$

The particles were inserted in the combustion chamber with the same temperature as the fluid (3400 K) and with an initial velocity of 50 m/s in order to avoid numerical problems by setting the velocity to zero. The mass fraction of the particles is 16%.

For the calculations that are going to be presented, the size and distribution of the particles was made according to what was provided by ESA:

- Minimum diameter: $3\ \mu m$
- Maximum diameter: $14\ \mu m$
- Average diameter: $6\ \mu m$

Two different approaches can be done:

a. The particle concentration is constant along the chamber section. Each diameter is present along the entire section.
b. The particles are considered to be linearly distributed by size, that is, the larger particles were closer to the centreline, whereas the smaller particles were further from the axis. This leads to a higher mass concentration near the axis.

3.2.3. Computational Model

The interaction of the particles with the flow was modelled with the use of a Lagrangian discrete phase model based on the Euler-Lagrange approach. The fluid phase is treated as a continuum by solving the Navier-Stokes equations, while the dispersed (solid) phase is solved by tracking a large number of particles through the calculated flow field. The particles can exchange momentum, mass and energy with the fluid phase. For these calculations, mass exchange was not considered since the particles are assumed to have the same size throughout the flow. The particle trajectories are computed individually at specified intervals during the fluid phase calculation.

As stated before, the Lagrangian discrete phase model can only be used if the solid phase occupies a small volume fraction (usually, lower than 10-12% [26]). A high mass percentage is acceptable as long as the volume fraction is small. This model is usually appropriate for the modelling of spray dryers, coal and liquid fuel combustion, and some particle-laden flows, but should not be used for the modelling of liquid-liquid mixtures, fluidized beds, or any application where the volume fraction of the second phase can't be neglected.

The particle trajectories are calculated by integrating over time the force balance described in section 2.3 also known as the Particle Equation of Motion. The trajectory can be given by

$$\frac{dx_p}{dt} = u_p \tag{37}$$

where x_p is the particle position and u_p is the instantaneous particle velocity.

The previous equation was discretized by an implicit and trapezoidal scheme. These discretization schemes are the most common since they consider most of the changes in the forces acting on the particles [26] and therefore are used as default by the software and were chosen for this work.

The drag coefficient was computed using Morsi and Alexander's spherical law [27], as defined in section 2.3.

3.2.4. Results

Effect of the Particle Size

The first set of calculations consisted of introducing a number of particles with constant size with a fraction of 16% of the fluid mass flow rate. To check the effect of the particle size the results presented afterwards consider the two extremes: minimum size (3 µm diameter) and maximum size (14 µm diameter). It is important to reinforce that in these cases the particle size is the same across the chamber section with a linear distribution of concentration.

The following figures present the changes in Mach number and temperature provoked by the particles. The upper part of the figures show the single-phase flow while the lower part show the two-phase flow with particles. Several changes are observed in both cases.

Minimum Size

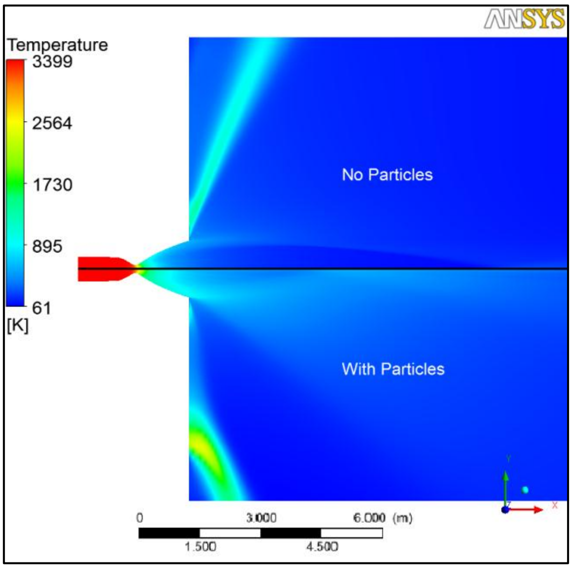

Figure 20 - Change in temperature for the minimum size particles.

Maximum Size

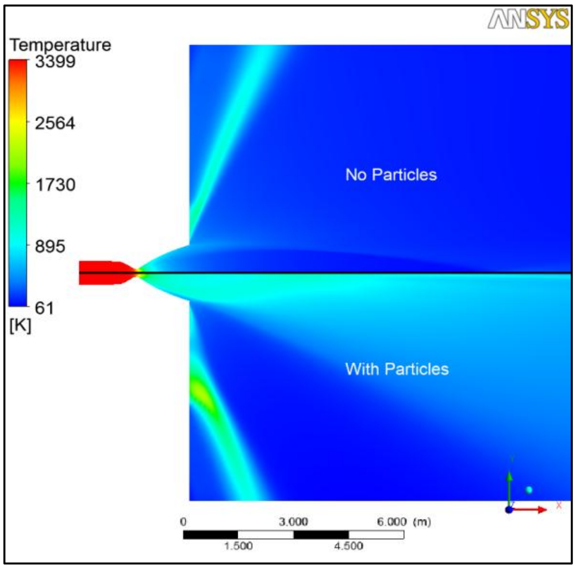

Figure 21 - Change in temperature for the maximum size particles.

Minimum Size

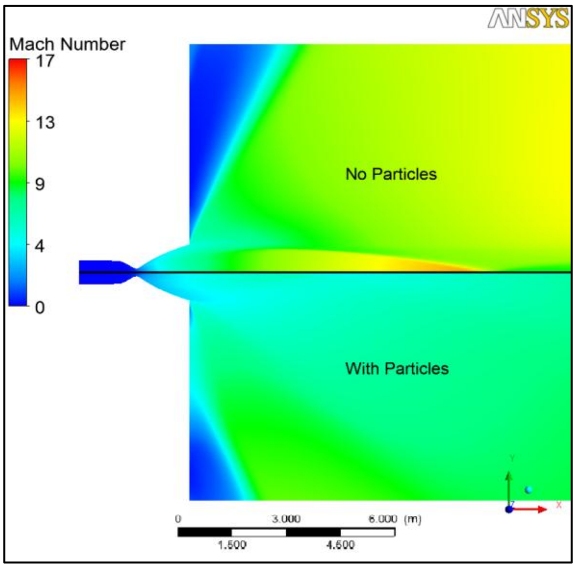

Figure 22 – Change in Mach number for the minimum size particles.

Maximum Size

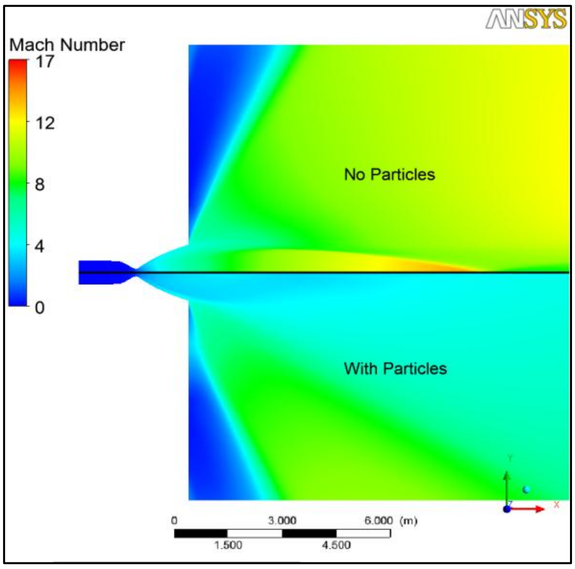

Figure 23 – Change in Mach number for the maximum size particles.

Finally, the plots presented next show the influence of the addition of the particles to the nozzle exhaust properties (temperature, pressure and velocity), which allow a better understanding of the particles influence in the nozzle performance parameters. The small noise near the centreline is due to the discrete phase model that was used to model the particles.

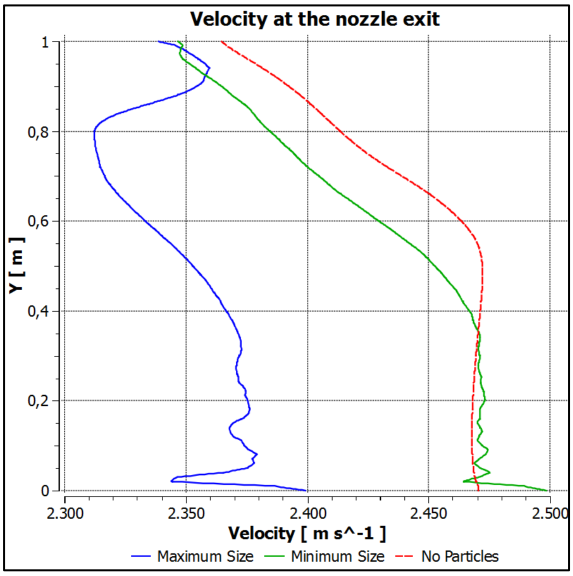

Chart 5 – Velocity at the nozzle exit for constant sized particles.

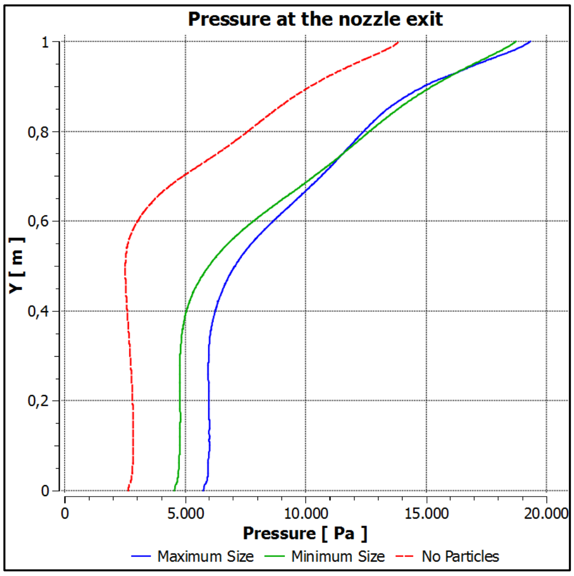

Chart 6 – Pressure at the nozzle exit for constant sized particles.

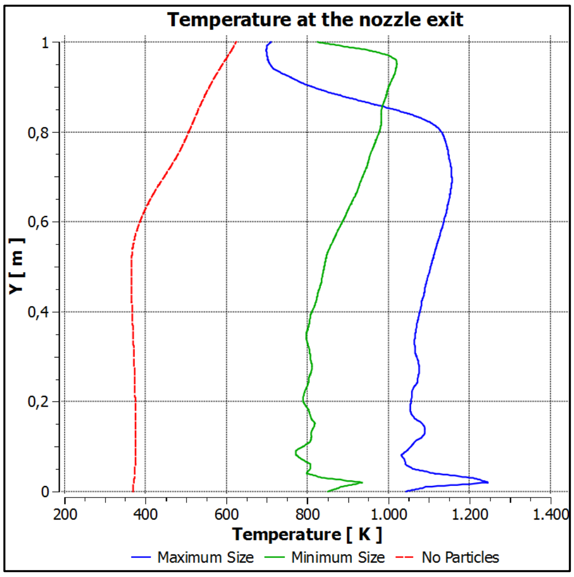

Chart 7 - Temperature at the nozzle exit for constant sized particles.

Effect of the Particle Distribution

The second set of calculations was made considering particles with a variable size ranging from 3 to 14 µm. Two calculations were made in order to check the influence of the particle distribution along the nozzle section. For the first case, the particles were distributed equally across the section while in the second case the bigger particles were concentrated in the middle.

The following figures show the temperature and Mach number distributions in the plume.

Distributed

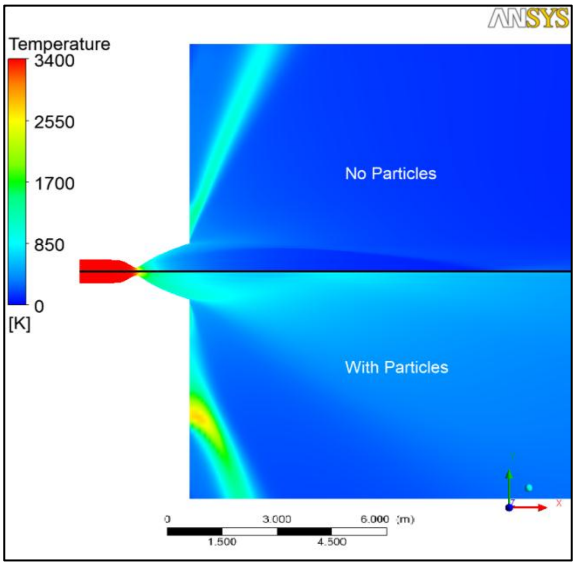

Figure 24 – Change in temperature for the distributed particles.

Concentrated

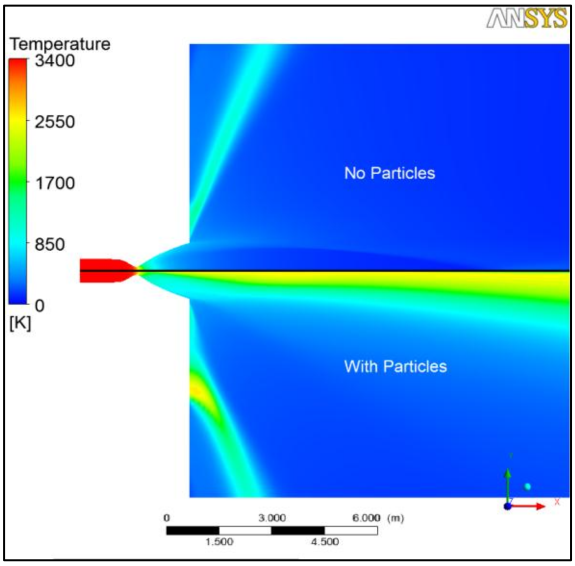

Figure 25 – Change in temperature for the concentrated particles.

Distributed

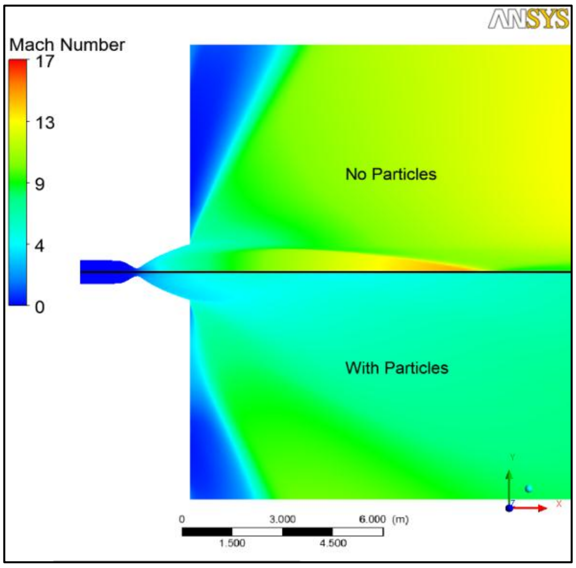

Figure 26 – Change in Mach number for the distributed particles.

Concentrated

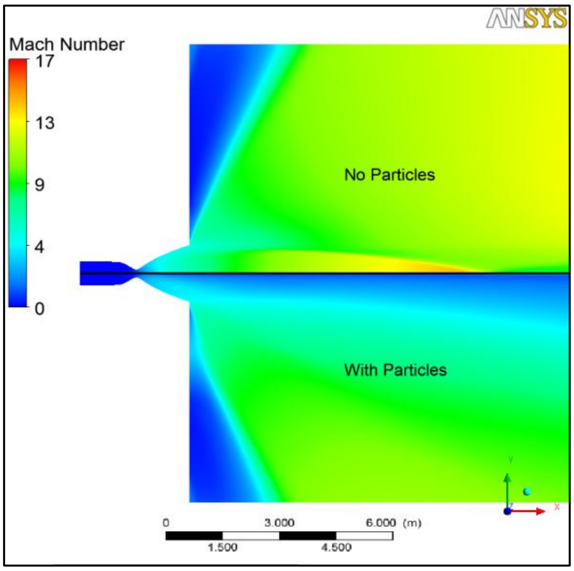

Figure 27 – Change in Mach number for the concentrated particles.

As before, the following charts present the properties of the flow at the nozzle exit, allowing for an estimation of the nozzle performance parameters.

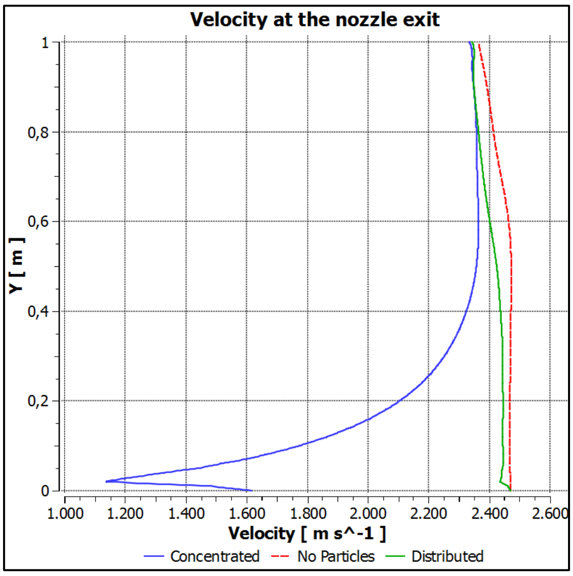

Chart 8 – Velocity at the nozzle exit for variable size particles.

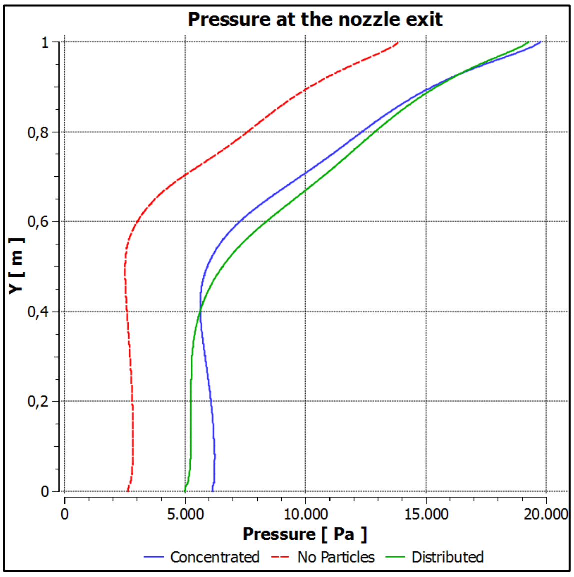

Chart 9 – Pressure at the nozzle exit variable size particles.

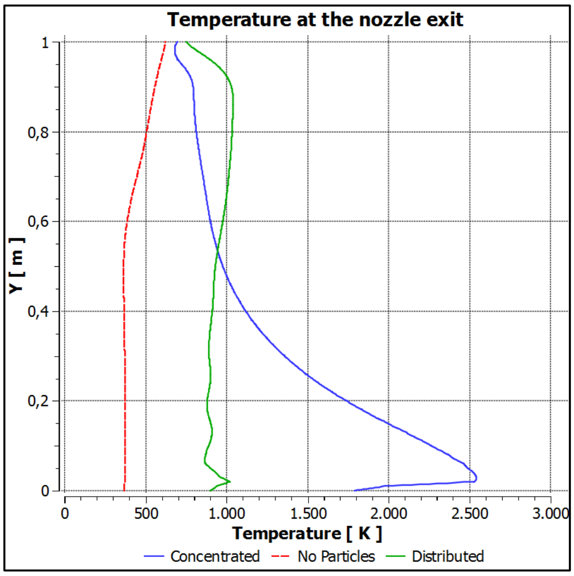

Chart 10 - Temperature at the nozzle exit for variable size particles.

Particle Trajectories and Concentration

Considering the case where the particles are equally distributed with variable sizes as the closest to the real distributions, the particle trajectories were computed and can be seen in the next figure.

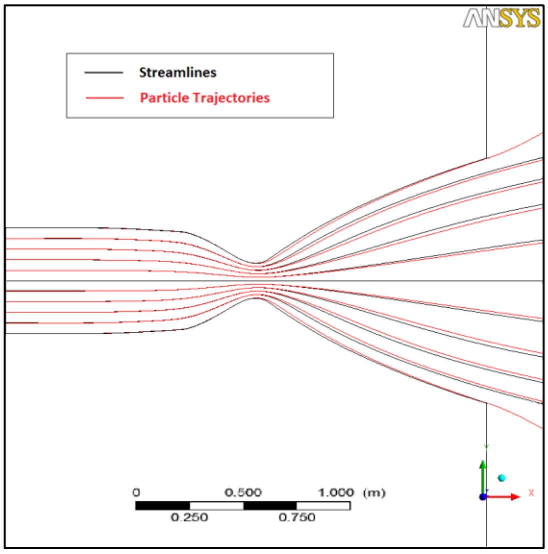

Figure 28 – Particle trajectories and flow streamlines

It is seen that the particles tend to follow the flow streamlines. The smaller particles, since they're lighter, are closer to the streamlines, whereas the bigger particles deviate more from the expected trajectories. In a case where the particles are all of bigger diameters, they become harder to turn, which can create a particle-free region close to the nozzle wall. This will also reduce the area of the external plume that is affected by the solid particles.

Figure 29 shows the plot of the particle mass concentration on the plume for the case where the particles range from 3 to 14 μm on a distributed pattern. The dark blue region corresponds to a very low particle concentration and can be assumed that it is not affected by particles. Comparing the particle concentration plot with the plume plot predicted on the previous subsection, it can be seen that the particles are confined to a thinner region, which means that the most open regions of the plume will most likely contain no solid particles. This is an important conclusion for the radiation study, as the higher temperatures caused by the particles affect mainly the core and its surroundings. This way, the extra radiation emitted by the hot particles will have less chances of reaching the payload.

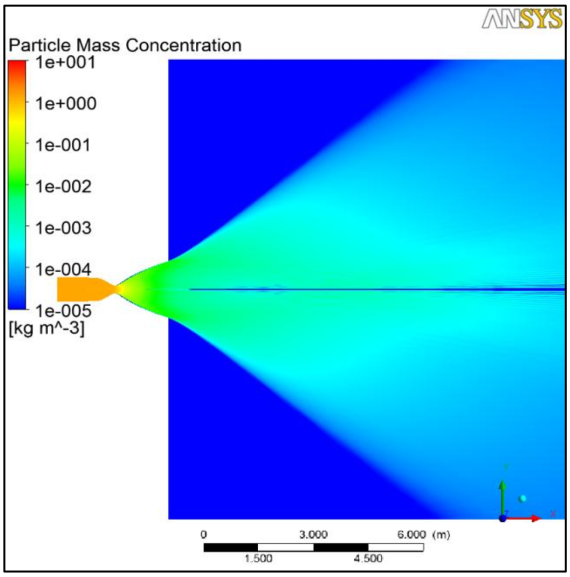

Figure 29 – Particle mass concentration plot.

3.2.5. Discussion

Numerical Errors

In all the simulations that include particles, it is observable that the region near the left outflow boundary doesn't present physically correct results. These errors have essentially two main sources. One of them is coming from the interaction with the boundary itself. Ideally, the left boundary should be far from the nozzle in order to avoid interference with the plume, which is the same as saying that the domain should be larger. The other problem is that that region contains extremely rarefied flow since the outflow is near vacuum. This way, the continuum approach is failing to obtain physically correct results.

Since these simulations aim to check the influence of the particles in the plume and the nozzle, the region affected by the numerical errors is not very important as there are no particles there (Figure 29). This way, it is assumed that the main regions of the plume, the ones that are affected by the introduction of the solid particles, are not directly affected by the interaction with the boundary and by the rarefied outflow.

3.2.5.1. Effect of the Particle Size

The introduction of the solid aluminium particles of any size has an immediate effect on the development of the flow. In both cases studied, it can be noticed that the shock diamond disappears as the flow decelerates. The overall plume temperature rises drastically, being higher the bigger the particles. However, the bigger particles tend to stick closer to the core which makes the outside regions of the plume not so hot. The evaluation of both these factors is fundamental to predict the amount of radiation that reaches the payload, as the radiated energy emitted by the core will be of higher intensity but less likely to reach the spacecraft than the one emitted by the cooler outside regions.

The charts presented also show a comparison of the properties at the nozzle exhaust. Introducing the particles raises the temperature from less than 400 K to 900 K (for the 3µm particles) or 1100 K (for the 14 µm particles), an increase of 125% and 175% respectively. The pressure is also raised more the bigger the particles are, whereas the velocity decreases as expected.

The thrust is also affected by the introduction of the particles. For the gaseous flow, the thrust can be calculated by the stream thrust technique presented before applied to the same control volume between the throat and the nozzle exit. However, it is important not to forget that the gas mass flow is now 16% lower since that fraction was replaced by solid particles. The momentum of the particles can be added to the equilibrium equation by an additional term

$$\int (\rho_{part}\mathbf{V}\cdot dA)\,\mathbf{V}$$

where ρ_{part} is the particle mass concentration and $\mathbf{V}$ is the particle velocity, which was considered to be the same as the fluid velocity although that's not true in reality.

The following table summarizes the differences between the thrust in the single-phase flow and the two cases with constant particle size.

Single-Phase	**3 µm**	**14 µm**
$183.6\ KN$	$179.88\ KN$	$169.5\ KN$

Table 5 – Thrust calculated for the flow with particles of the same size.

As expected, the introduction of the particles leads to a momentum loss which leads to a loss in thrust. It is also clear that the bigger particles tend to decelerate the flow more, reducing the thrust even more. This is one of the disadvantages of adding the particles, but they are still essential to improve the rocket general performance, so this influence must be overcame.

Effect of the Particle Distribution

The distribution of the particles is a factor that is extremely hard to predict. Although some studies have been done before, it is always safer to get experimental data. By analysing the plots before, it is possible to conclude that a good estimation of the particle effect can't be obtained if the distribution is wrongly estimated.

If the particles are assumed to be distributed according to their size, with bigger particles closer to the centreline due to their weight, then there will be a higher concentration in that region, leading to harsher changes on the resulting plume. On the other hand, if the particles present a random distribution, where every size is present along the entire section, then the concentration is approximately the same and the changes provoked by them are softer.

As before, the thrust was estimated and the results are summarized in the following table:

Single-Phase	**Distributed**	**Concentrated**
$183.6\ KN$	$176.22KN$	$172.26\ KN$

Table 6 – Thrust calculated for the flow with particles of variable sizes.

Once again, the particles tend to reduce the thrust produced. Due to the concentration near the centreline that highly slows down the flow in that region, it is clear that the decrease in the thrust is higher for the concentrated particle distribution.

General Discussion

The high altitude plume suffers several physical and chemical changes when the solid particles are included. The qualification of these changes provides a tool to find the optimum percentage of aluminium that should be added to the propellant mix.

The previous calculations give a general overview of the effect that the particles may have in the thermodynamic properties of the flow and in the nozzle performance. It was seen that the size and the distribution of the particles can have a major influence in the resulting plume, proving once more the importance of an accurate prediction of these factors. It is important to note that the analysis was made with aluminium instead of alumina since the chemical reactions were not considered, which includes the oxidation of the aluminium. The variation of the properties is shown here qualitatively since the complex mixture of gases that really exists in the combustion chamber would greatly increase the computational time needed.

The influence of the particles in the plume temperature should be highlighted due to the influence on the emission of radiation by the plume. The higher temperatures should increase the amount of thermal radiation that can be received by the spacecraft. Therefore, the particles can’t be neglected when simulating the plume. The larger the particles, the more the temperature will raise, making it important once more to know their size and distribution.

The following can be concluded from these analyses considering the introduction of the solid aluminium particles:

- The overall temperature of the plume rises, which increases the thermal radiation emitted.
- The overall velocity decreases, which leads to a drop in the thrust produced by the nozzle.
- The smaller the particles, the smother the changes are. Bigger particles also tend to concentrate more near the centreline as they’re heavier.
- The distribution of the particles and of their sizes can cause different responses on the plume, making it important to know accurately how are the particles distributed in the chamber.

4. LOW ALTITUDE PLUME

While the effects in high altitude plumes are important because of the radiation concerns due to the highly open plume, in low altitude the main problem caused by the increase in temperature comes with the chemical reactions that can happen with the atmosphere that is no longer rarefied, increasing the reaction rate. The combustion products of a solid propellant rocket can be toxic by themselves, but once they react with the atmosphere, high amounts of carbon monoxide and dioxide are formed. This process is sometimes called "afterburning" as it occurs after the combustion itself and it occurs in the atmosphere.

4.1. Assumptions

The assumptions used to model the low altitude plume were the same as used before, but the model is more accurate for this case.

The continuum approach is now valid for the whole flowfield are there are no rarefied areas due to the lower altitude and higher ambient density.

4.2. Boundary Conditions

The boundary conditions of the combustion chamber and the nozzle are the same as the ones used in the high-altitude calculation, as well as the gas properties. The outflow conditions were changed in order to correspond to the increased pressure and temperature found at lower altitudes.

Gas properties (Air):

- $c_p = 1006.43\, J/(kg \cdot K)$
- $k = 0.0242\, W/(m \cdot K)$
- Molar mass - $M = 28.966\, kg/kmol$

Combustion chamber:

- $T_0 = 3401\, K$ (expected temperature in the chamber after the combustion)
- $p_0 = 74\, bar$

The velocity inside the chamber is very small. Therefore, these conditions correspond to the flow stagnation properties.

Nozzle wall:

- Slip wall with no shear stress.

The slip wall condition guarantees that no boundary layers will be taken into account in the viscous calculation.

Outflow and ambient conditions:

The low altitude calculations were based on an operating point provided by Avio [34].

- $T = 220\ K$ (temperature was not provided, however, this value is a typical value for this altitude assuming standard atmosphere [1])
- $p = 5400\ Pa$
- $M = 3.4$

4.3. Computational Model

The computational model used for these calculations can be exactly the same as the one used before, including the mesh. The numerical errors that occurred in the boundary are expected to be reduced or even eliminated as the two main causes are no longer present, that is, the rarefaction and the interaction with the domain boundaries.

The convergence process was shown to be much faster due to the smaller pressure and density gradients, which proves that any future analysis will be easier to test and to solve in the low altitude case.

The introduction of the particles is also done the same way as before, considering the most likely case of size and distribution. The particles are assumed to be evenly distributed with sizes ranging from 3 to 14 µm.

4.4. Results

Figure 30 and Figure 31 show the low altitude plume with and without particles just like was done before for the high-altitude simulation. The same phenomena are observed: the particles decelerate and heat up the flow, which makes the Mach diamond disappear.

The low altitude plume immediately shows much lower velocities than the high altitude one, as can be seen on Figure 32. This is caused by the increase in the ambient pressure that reduces the need of an expansion outside the nozzle, dropping the acceleration. As for the other properties, the most important one to consider is the temperature due to the radiation and chemical problems that come with it. As the exhaust plume is now surrounded by a hotter outflow and it is smaller and more concentrated, the flow coming from the nozzle finds it harder to cool down as can be seen in Figure 33.

Mach Number

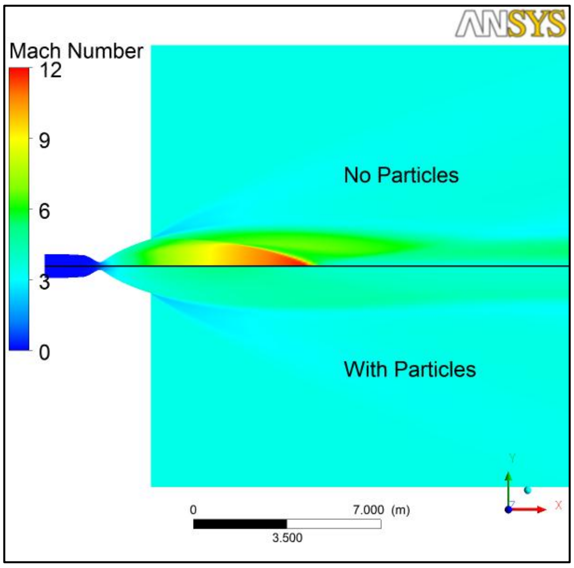

Figure 30 – Mach number plot for the low altitude plume.

Temperature

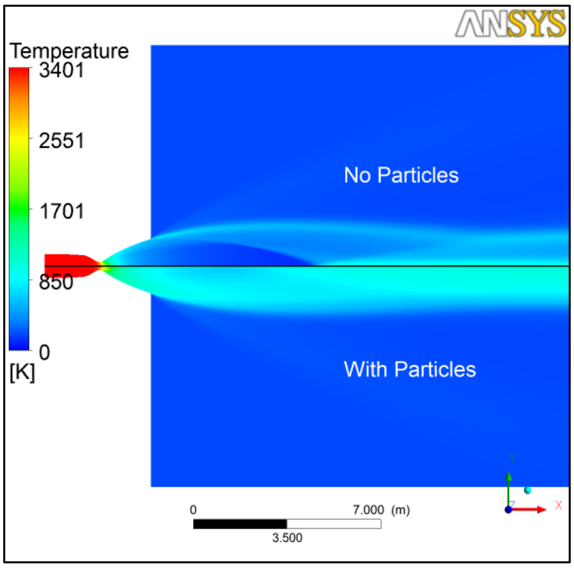

Figure 31 – Temperature plot for the low altitude plume.

Mach Number

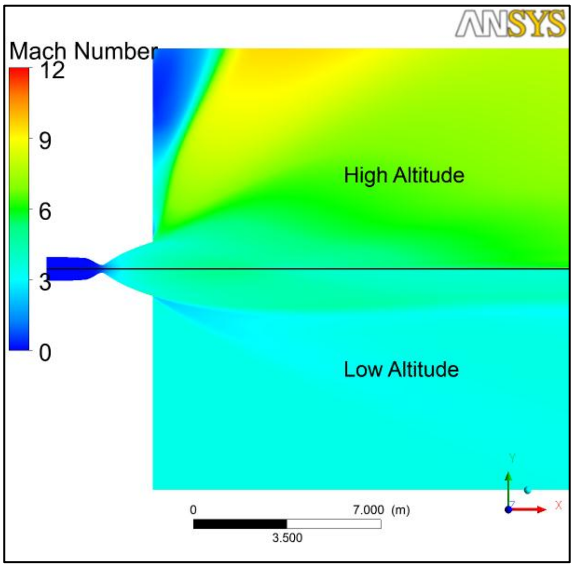

Figure 32 – Mach number plot for the low altitude plume.

Temperature

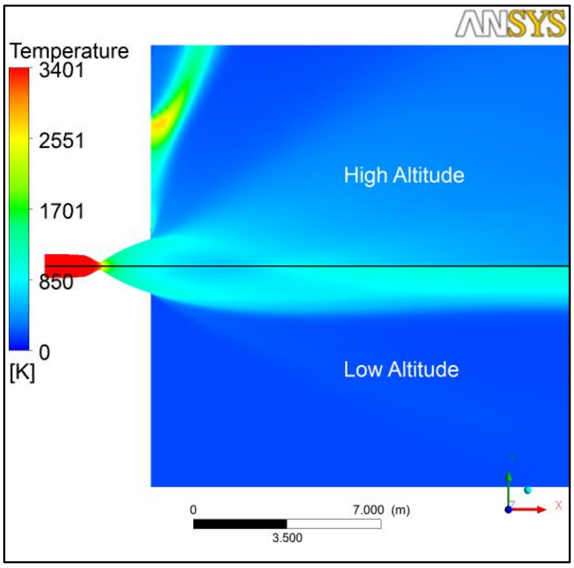

Figure 33 – Temperature plot for the low altitude plume.

The particle mass concentration (Figure 34) plot shows an important difference in terms of the region influenced by the particles. In low-altitude plumes, since the expansion is smoother, the particles don't need to turn as much, therefore affecting the entire plume. On the other hand, high altitude plumes have a relatively large particle-free region.

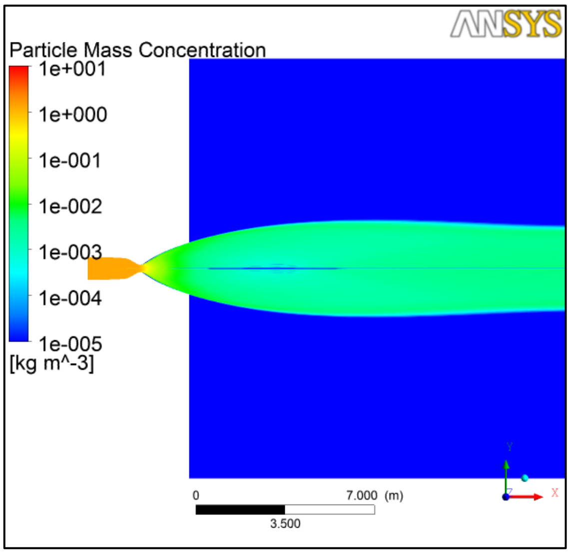

Figure 34 – Particle mass concentration plot for the low altitude plume.

4.5. Discussion

General Discussion

The main changes that come with the altitude variation are the conditions of the atmosphere. Lower altitudes have higher pressure, density and temperature, and that makes them a lot easier to study. In a computational way, the smaller gradients help with the convergence process and speed up the simulations, allowing for more solution improvements. On the other hand, the higher density eliminates the need of a rarefied flow code, which eliminates one of the major problems found in the high altitude plume studied before. For this reason, the solution also has better quality. As the opening angle is now smaller, the interaction between the plume and the boundary is very small and the presented graphics show a much smoother plot of Mach number and temperature, without any visible numerical errors.

The nozzle performance also has a small change with the altitude. The properties at the nozzle exit are the same, because the flow is still underexpanded and the geometry is unchanged (like it was reviewed back in Chapter 2). However, the high altitude plume wastes immense amounts of energy to expand the flow until near vacuum, which means that a big part of the combustion energy is lost to space. As stated before, the ideal conditions would need an ambient pressure equal to the nozzle exit pressure, but that is impossible to obtain without changing the nozzle geometry. Therefore, the majority of the nozzles end up losing some efficiency in order to be able to operate in conditions other than the design ones. To avoid a big loss in higher altitudes, some launchers have multi stage rockets that are designed for different altitudes.

Thrust Estimation

Like before, let's now estimate the thrust provided by the rocket under these specific conditions. First, let's consider the single-phase flow and control volume similar to the one used before for these calculations, which has the throat as an inlet and the nozzle exit as an outlet.

Recurring once again to the stream thrust averaging technique we obtain:

$$F_{throat} = 609\ KN$$

$$F_{exit} = 792.6\ KN$$

$$\boldsymbol{F_{net} = 183.6\ KN}$$

These results happen to be the same as the ones obtained for the high-altitude single-phase plume. This is expected on a nozzle that has no varying geometry. Since the expansion ratio and the throat area are the same, as well as the chamber conditions, the only changes from the previous case are in the external pressure and temperature. This way, the force acting on the nozzle walls is the same in both cases for the single-phase flow.

For the two-phase flow, the same procedure can be followed. Now let's take into account the momentum of the particles like was done before. The thrust obtained has a value of:

$$\boldsymbol{F = 176.22\ KN}$$

This value is comparable to the high-altitude case where the particles are distributed with a variable size. It is clear that, like explained before, the external properties of the flow do not change the thrust produced by the rocket.

5. CONCLUSIONS

From the results obtained and the analysis that was done there are several important conclusions that can be taken to launch the basis for the future developments for this project.

- The influence of the solid particles can't be neglected under any circumstance as their influence in the gaseous flow is very high, raising the temperature and lowering the velocity. The nozzle performance is also highly affected.
- The type, shape, size and distribution of the particles affect the way they behave in the plume. It is important to know with some accuracy the real conditions of the particles.
- There are some numerical errors leading to physical inconsistencies that are due to the interaction with the boundaries and to the rarefied flow areas.
- Several improvements are needed in order to obtain a more accurate solution. However, these results provide a good initial estimation of the effect of the particles in the plume.

6. FUTURE DEVELOPMENTS

As explained and discussed throughout the report there are several important developments and changes that shall be done in order to improve the solutions and further confirm the conclusions which can be summarized by:

- Improved geometry;
- Improved order of the discretization methods;
- Use of a rarefied gas solver method like DSMC;
- Use of the real composition of the gaseous plume.

Besides this, further developments can be done to take advantage from the results obtained and to allow the reaching of the final goal of the project.

- Addition of the models for the chemical reactions occurring on the chamber and the plume.
- Addition of the radiation models that allow the estimation of the radiation emitted by the plume and whether it reaches the payload or not.

Improved geometry

The geometry used for the calculations done on this work was defined in order to observe the behaviour of the plume exiting the nozzle and was limited to provide a faster solution. In a future computation, the flow domain should be enlarged, both in width and height. The nozzle should also be converted into a solid body representing the entire launcher and located somewhere inside the domain, in order to avoid interferences with the boundary conditions like what happened in the cases presented in Chapter 4. Ideally, the domain should be built closely to what is represented on Figure 35.

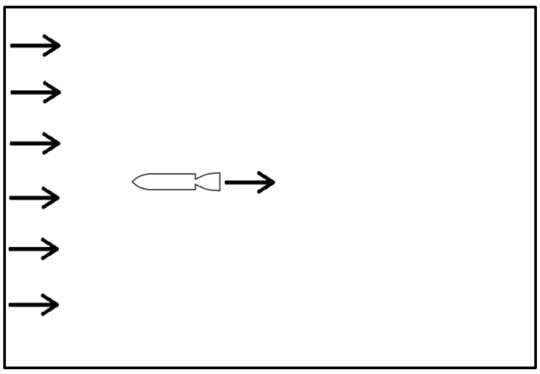

Figure 35 – Hypothetical domain to be used in a future calculation.

Improved order of the discretization methods

The spatial and temporal discretization methods used before tried to achieve a fast solution in the first place and allow a good convergence process. Therefore, their accuracy is somehow limited by their simpler algorithms. In order to improve the accuracy of the solution some other discretization methods can be used.

The first order upwind scheme used throughout this work provides good accuracies if the flow is aligned with the mesh. In order to avoid errors associated with this, second or higher order schemes may be used. While the higher-order scheme may result in greater accuracy, it can also result in convergence difficulties and instabilities at certain flow conditions, which was already verified for the given flow and boundary conditions. The convergence was found to be a lot harder to obtain with the second order discretization, which was the reason it was not used in the final results. However, it will be necessary to use a higher order discretization method in order to help correcting the physical inconsistencies that some of the plots show.

Use of a rarefied gas solver

As explained before, the continuum approach is not valid for certain regions of the plume. In the most rarefied regions there a need for a different solver that solves the equations for rarefied flows like the Boltzmann equation. One of the most common methods for rarefied flows is the Direct Simulation Monte Carlo method (DMSC). The DSMC method is a model developed by Bird [35] that solves the Boltzmann equation by discretising the phase space by using for example, finite differences. It was developed to be used in rarefied flows of high Knudsen number, however, nowadays, it is possible to use it for continuum flows and compare it with the Navier-Stokes solutions like it was done by several authors [20] [21] [22].

The DSMC method works by dividing the space in elementary cells, each one of them is filled with some sample particles representative of all the particles that would be in that cell. These sample particles move with different speeds and are allowed to interact and collide. The collision parameters are taken from a statistical model.

This model is highly used nowadays as its flexibility allows it to adapt itself to many situations and many types of molecules. There are obviously some errors that come with the statistical models used for the collision parameters, however, according to [31], they can be controlled and reduced by increasing the number of sample particles.

For high altitude plumes, the best model in theory would be a hybrid between a Navier-Stokes solver and a DSMC solver that uses the required model based on the local Knudsen number, like it was proposed by Selezneva et al. [20]. This kind of implementation is however very difficult to achieve as the coupling between the models can be widely expensive economically and time wise. The hybrid solver would also need a criterion for the failure of the NS equations [20] which is sometimes hard to obtain. For this reason, a NS solver should guarantee a fairly accurate solution in order to get the influence of the radiation. If one needs to get detailed information about the interaction between the plume and the outflow, then a model based on the DSMC method should be added.

Use of the real composition of the plume

The calculations done for this work were based on a mixture of air and aluminium. However, knowing the original fuel composition (HTPB, AP and Aluminium) it is possible to obtain the exact percentages of each combustion product in the combustion chamber, after the combustion. Since there are still reactions occurring in the flow, for a better accuracy there should be added chemical reaction models, therefore unfreezing the flow. This requires a very hard to obtain set of information like the Arrhenius constants for every single reaction, which drastically increases the solving time and should be done only in the final calculation, to provide the better result possible.

Introduction of the radiation models

Once the plume solution is obtained, radiation models can be added. The main goal for this future work is to obtain the radiation pattern emitted by the hot gaseous plume and to check its influence in the payload. Modelling radiation from gases is very difficult as the emissivity properties depend on a lot of factors like pressure, temperature, concentration and molecular species.

BIBLIOGRAPHY

[1] G. P. Sutton and O. Bilbarz, Rocket Propulsion Elements, 8th Edition ed., USA: John Wiley and Sons, Inc., 2010.

[2] A. Davenas, “Solid Rocket Motor Design,” in *Tactical Missile Propulsion - Progress in Astronautics and Aeronautics*, Chapter 4, vol. 170, G. E. Jensen and D. W. Netzer, Eds., AIAA, 1996.

[3] N. Kubota, “Survey of Rocket Propellants and Their Combustion Characteristics,” in *Fundamentals of Solid-Propellant Combustion - Progress in Astronautics and Aeronautics*, vol. 90, K. K. Kuo and M. Summerfield, Eds., AIAA, 1984.

[4] C. Boyars and K. Klager, Propellants: Manufacture, Hazards and Testing, vol. 88, Advances in Chemistry - American Chemical Society, 1969.

[5] J. M. Burt, “Monte Carlo Simulation of Solid Rocket Exhaust Plumes at High Altitude,” PhD Dissertation, University of Michigan, 2006.

[6] S. C. Hunter, S. S. Cherry, J. R. Kliegel and C. H. Waldman, “Gas-Particle Nozzle Flows with Reaction and Particle Size Change,” in *AIAA 19th Aerospace Sciences Meeting*, 1981.

[7] W. S. Bailey, E. N. Nilson, R. A. Serra and T. F. Zupnik, “Gas Particle Flow in an Axisymmetric Nozzle,” *ARS Journal,* vol. 31, no. 6, pp. 793-798, 1961.

[8] R. Matsuzaki, “Quasi-one-dimensional aerodynamics with chemical, vibrational and thermal nonequilibrium,” *Japan Society for Aeronautical and Space Sciences,* vol. 30, pp. 243-258, 1988.

[9] J. R. Kliegel and G. R. Nickerson, “Flow of Gas-Particles Mixtures in Axially Symmetric Nozzles,” TRW Space Technology Labs, Los Angeles, 1961.

[10] I. Chang, “One and Two-Phase Nozzle Flows,” *AIAA Paper,* vol. 80-0272, p. 1-17, 1980.

[11] C. J. Hwang and G. C. Chang, “Numerical Study of Gas-Particle Flow in a Solid Rocket

Nozzle,” *AIAA Journal,* vol. 26, no. 6, pp. 682-689, 1988.

[12] D. E. Coats, N. S. Cohen, J. N. Levine and D. P. Harry, “A computer program for the prediction of solid propellant rocket motor performance, Volume 1,” Ultrasystems Inc, 1975.

[13] G. Morrell, “Critical Conditions for Drop and Jet Shattering,” *NASA Techincal Note,* vol. 677, 1961.

[14] R. W. Hermsen, “Aluminium Oxide Particle Size for Solid Rocket Motor Performance Prediction,” *Journal of Spacecraft and Rockets,* vol. 18, no. 6, pp. 483-490, 1981.

[15] H. Fein, “A Theoretical Model for Predicting Aluminium Oxide Particle Size Distribution in Rocket Exhausts,” *AIAA Journal,* vol. 4, no. 1, pp. 92-98, 1966.

[16] R. Jenkins and R. Hoglund, “A Unified Theory of Particle Growth in Rocket chambers and Nozzles,” *AIAA Paper,* no. 69-541, 1969.

[17] F. E. Marble, “Droplet Agglomeration in Rocket Nozzles Caused by Particle Slip and Collision,” *Astronautica Acta,* vol. 13, pp. 159-166, 1967.

[18] T. H. Nack, “Theory of Particle Agglomeration, Mean Size Determination and Chamber Coagulation in Rocket Motors",” *Proceedings of the AFRPL Two-Phase Flow Conference,* vol. I, p. 103, 1967.

[19] C. T. Crowe and P. G. Willoughby, “A Study of Particle Growth in a Rocket Nozzle,” *AIAA Journal,* vol. 5, pp. 1300-1304, 1967.

[20] S. E. Selezneva, M. I. Boulos, M. C. M. v. d. Sanden, R. Engeln and D. C. Schram, “Stationary supersonic plasma expansion: continuum fluid mechanics versus direct simulation Monte Carlo method,” *Journal of Physics D: Applied Physics ,* pp. 1362-1372, 2002.

[21] I. D. Boyd, P. F. Penko and D. L. Meissner, “Numerical and experimental investigations rarefied nozzle and plume flows of nitrogen,” in *AIAA 26th Thermophysics Conference*, 1991.

[22] S. Pal, S. Dey and T. Miebach, “Numerical simulation of a dual-source supersonic plasma

jet expansion process: continuum approach," *Journal of Physics D: Applied Physics,* vol. 40, no. 10, p. 3128–3136, 2007.

[23] G. V. Candler, D. A. Levin, J. Brandenburg, R. Collins, P. Erdman, E. Zipf and C. Howlett, "Comparison of Theory with Plume Radiance Measurements from the Bow Shock Ultraviolet 2 Rocket Flight," *AIAA Paper 92-0125,* 1992.

[24] P. W. Erdman, E. Zipf, P. Espy, C. Howlett, D. A. Levin and G. V. Candler, "In-Situ Measurements of UV and VUV Radiation from a Rocket Plume and Re-entry Bow Shock," *AIAA Paper 92-0124,* 1992.

[25] J. D. Anderson, Modern Compressible Flow: With Historical Perspective, USA: McGraw-Hill, 1982.

[26] Fluent® Inc., "FLUENT 13.0 User's Guide," 2011.

[27] S. A. Morsi and A. J. Alexander, "An Investigation of Particle Trajectories in Two-Phase Flow Systems," *Journal of Fluid Mechanics,* vol. 55, no. 2, pp. 193-208, 1972.

[28] S. V. Apte, K. Mahesh and T. Lundgren, "A Eulerian-Lagrangian model to simulate two-phase/particulate flows," *Center for Turbulence Research - Annual Research Briefs,* pp. 161-171, 2003.

[29] F. S. Simmons, Rocket Exhaust Plume Phenomenology, California: The Aerospace Corporation, 2000.

[30] "Knudsen number," [Online]. Available: http://en.wikipedia.org/wiki/knudsen_number. [Accessed 1st September 2011].

[31] H. Struchtrup, Macroscopic Transport Equations for Rarefied Gas Flows, Germany: Springer, 2005.

[32] "Sutherland's Law," [Online]. Available: http://www.cfd-online.com/Wiki/Sutherland_law. [Accessed 23rd June 2011].

[33] D. H. Wong, ESA/AOES.

[34] V. Ferrara, F. Paglia, A. Mogavero, M. Genito and M. Bonnet, “Ground to Flight Extrapolation of SRM Radiative Loads,” in *Proceedings of the 7th European Symposium on Aerothermodynamics - European Space Agency*, Noordwijk, Netherlands, 2011.

[35] G. A. Bird, Molecular Gas Dynamics and the Direct Simulation of Gas Flows, Clarendon Press, 1994.